GERMAN - MONGOLIAN INSTITUTE FOR RESOURCES AND TECHNOLOGY

The present work was submitted to the Faculty of Engineering

Assessment of Land Use effects on Tuul River surface water Quantity and Quality

Bachelor Thesis

by

Bolorchimeg Turkhuu

Study Program	Environmental Engineering
Supervisor 1 / Examiner 1	Dr. Ariuntuya Tserendorj
Supervisor 2 / Examiner 2	Ph.D. Byambakhuu Ishgaldan

Ulaanbaatar/Nalaikh, 2022

Statutory Declaration

Turkhuu, Bolorchimeg	15012217010518
Last Name, First Name	Student ID Number

I hereby affirm in lieu of an oath that I provided the submitted bachelor thesis

ASSESSMENT OF LAND USE EFFECTS ON TUUL RIVER SURFACE WATER QUANTITY AND QUALITY

I did not use any sources other than those stated. In case that the work is additionally submitted on a data medium, I declare that the written and the electronic form are completely identical. The work was not submitted in the same or similar form to any examination authority.

Ulaanbaatar/Nalaikh, 05/16/2022	
Place, Date	Signature

Table of Contents

List of Figures

List of Tables

List of abbreviation

GDP: Gross Domestic Product

SWAT: Soil and Water Assessment Tool

LULC: Land Use and Land Cover

USDA-ARS: United States Department of Agriculture and Agricultural Research Service

HRU: Hydrologic response unit

DEM: Digital Elevation Model

CN: Curve number

SWAT-CUP: SWAT-Calibration and Uncertainty Programs

PPU: Percent Prediction Uncertainty

NSE: Nash-Sutcliffe efficiency coefficient

PBIAS: Percentage bias

ET: Actual evapotranspiration

PET: Potential evapotranspiration

TSS: Total suspended solid

Acknowledgement

The bachelor thesis period was full of great experiences. During the thesis study, I received enormous support from many people. Without their support, the bachelor thesis would have been more difficult to overcome throughout the research and the writing of this thesis. It is my pleasure to express acknowledgement to the people who have supported me.

I would like first to express my sincere gratitude to my first supervisor, Dr. Ariuntuya Tserendorj for her continuous support of my thesis study and research, and for her useful advice during the whole time. She always discussed with me whenever I asked for a consultation and advised me on how to improve my thesis writing.

Also, I would like to express my warmest gratefulness to my second supervisor, Ph.D. Byambakhuu Ishgaldan for his patience, enthusiasm, countless suggestions, and introducing me to the use of SWAT model. I am very glad to him for giving me an opportunity to do research about hydrological modeling and to learn the concepts of modeling from the beginning. His encouragement made me remain focused to finish this study. Besides the thesis study, he has always welcomed me to discuss about my future plan and helped me in seeing life and science in their full depth.

Lastly, I want to sincerely thank my parents for loving me unconditionally, and supporting me in all of my pursuits. With their endless encouragements, I can stay confident in all my decisions.

Abstract

The Tuul river basin is a unique region in that it covers only 3.2% of Mongolian territory, but 48% of Mongolian total population lives in Ulaanbaatar. Also, 66.5% of the Mongolian total GDP was produced within this river basin in 2020. Land-use changes due to the expansion of urbanization can pose a threat to downstream ecosystems of the Tuul river, particularly soil and water quality, leading to an increase in surface runoff and nutrient loads. The main purpose of this study is to evaluate the impacts of land-use and land cover changes in discharge and water quality in the upper part of the Tuul river basin between 2010 and 2019. Land use/land cover changes, digital elevation model, soil, and meteorological data were used as an input data for the Soil and Water Assessment Tool (SWAT) to simulate streamflow and water quality. The model's performance was determined by statistical parameters including Nash-Sutcliffe efficiency coefficient (NSE), correlation coefficient (*r*), and percentage bias (PBIAS). Furthermore, prediction uncertainty was measured using the p-factor and r-factor. The values of NSE (0.56 and 0.66) and *r* (0.77 and 0.82) for calibration and validation periods at a daily time scale showed that the SWAT model could be used to simulate the discharge. The results of calibrated model showed the increase in surface runoff, and loads of nitrate and phosphorus due to rapid urbanization in the Tuul river basin. The outcomes of the study can be useful in understanding water management strategies and making more appropriate land management decisions and practices.

1. Introduction

Arid ecosystems, which are characterized by a lack of rainfall and high evapotranspiration, constitute over one-third of the Earth's terrestrial surface (1). Water is the significant governing factor for vegetation growth in arid and semiarid regions such as Mongolia (2). Surface water accounts for 87 percent and groundwater makes up the remaining 13 percent of the total water resources of Mongolia (3). Mongolia is divided into 29 river basins (Figure 1); each of them varies water resources, regime, water use, and pollution issues depending on the geographical situation, natural zones, climatic conditions, population density, urban and major economic sectors (4). The Tuul river is one of the longest rivers among 29 river basins. The basin covers only 3.2 percent of Mongolia's territory; nevertheless, about 48 percent of Mongolian population lives in Ulaanbaatar and about 66.5 percent of its gross domestic product is produced in Ulaanbaatar. Ulaanbaatar city supplies drinking and industrial water usage from the groundwater resource of the Tuul river valley. The Tuul river basin has an estimated groundwater resource of approximately 641 million m^3 per year and a surface water resource of around 1.59 km^3 per year (4). As a matter of fact, in recent years the water quality of river and perennial streams in Mongolia is deteriorating due to global warming, and changes in land use, such as the transitions from pasture land to urban land and mining (5).

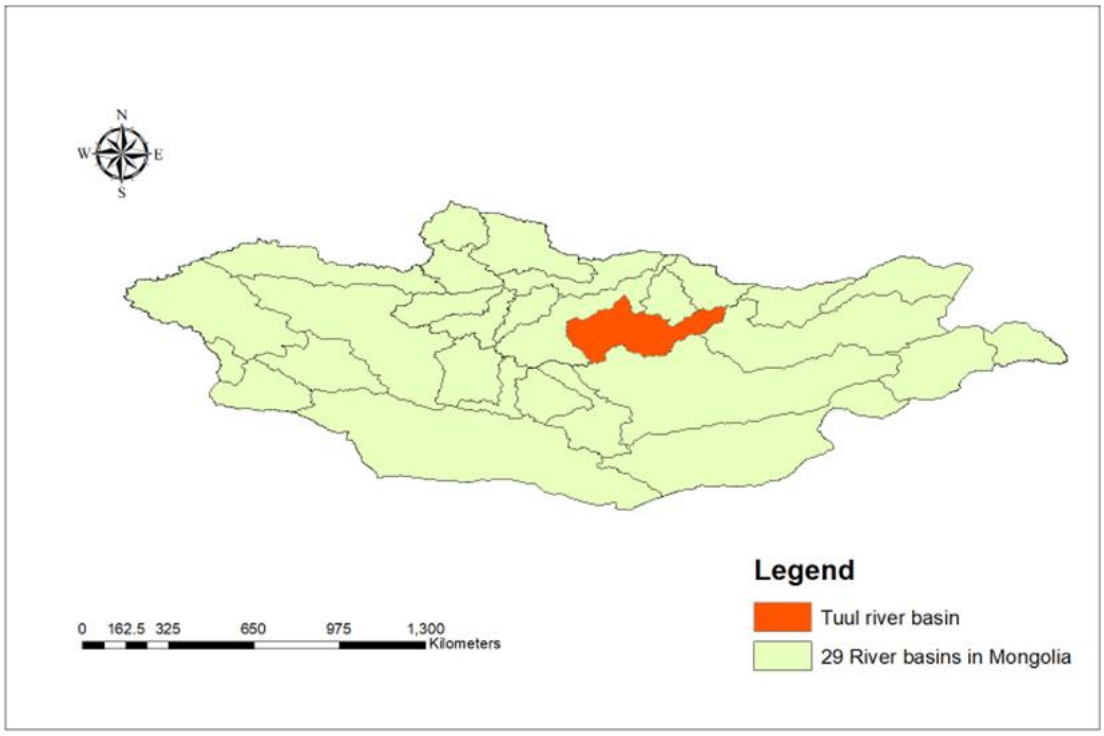

Figure 1. Location of Tuul River Basin

The Tuul river basin has a high concentration of population, which is the most economically viable region in Mongolia. Thus, the importance of this basin tends to increase in the future. Unfortunately, due to rapid population growth and urbanization within the upper part of the Tuul river basin, changes in land use pattern and climate continue to have a remarkable impact on the surface water quantity and quality of the Tuul River (6).

The Tuul river flows through densely populated Ulaanbaatar city, the capital of Mongolia. The Ulaanbaatar area covers only 0.3 percent of Mongolian territory, although according to 2020 population statistics, 47.6 percent of the total population has been living there (7). During the last two decades, the number of populations in Ulaanbaatar has increased by approximately 28 percent (Figure 2).

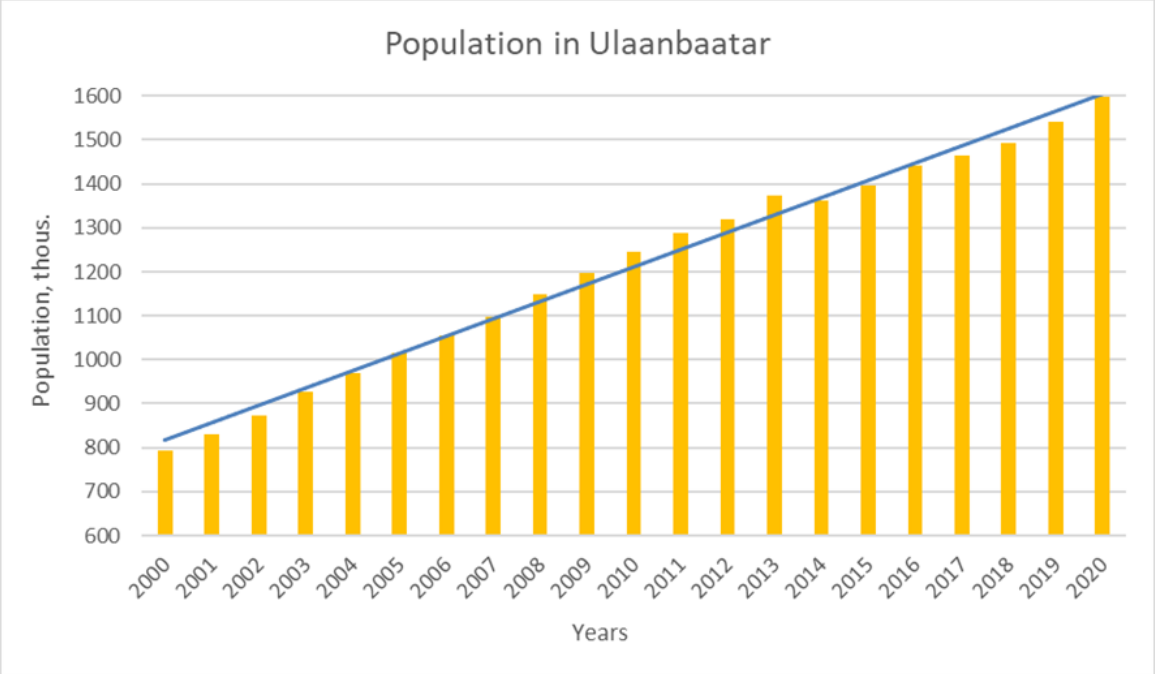

Figure 2. Population changes in Ulaanbaatar

As shown in Figure 3, 66.5 percent of Mongolian total Gross Domestic Product (GDP) was produced within the Tuul river basin in 2020. GDP produced in the basin has increased year by year dramatically. For instance, GDP produced in Ulaanbaatar in 2020 has quadrupled since 2010.

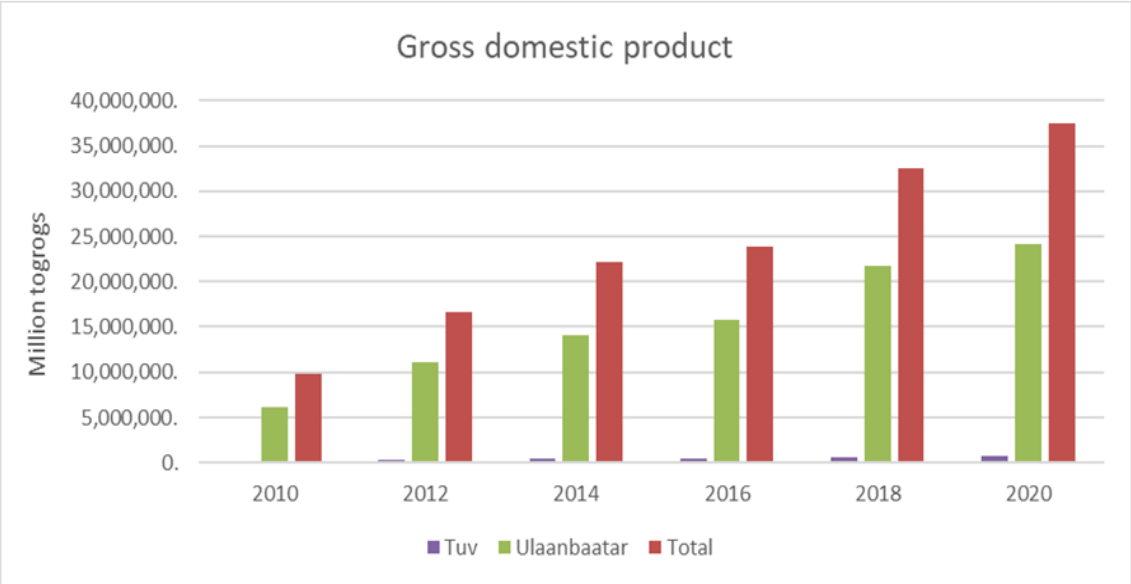

Figure 3. The amount of GDP produced in the basin

According to the report of the unified territory of Ulaanbaatar, pasture land accounts for 4560.9 thousand hectares, or 91.2 percent of the total area, and the area of agriculture, hay, settlements, forests, water body, and roads covers between 0.3 and 6.8 percent (8). Urban areas have expanded by 10 percent since 2003 and the area of pasture land has decreased slightly within the basin, the administration area of Ulaanbaatar city (Figure 4).

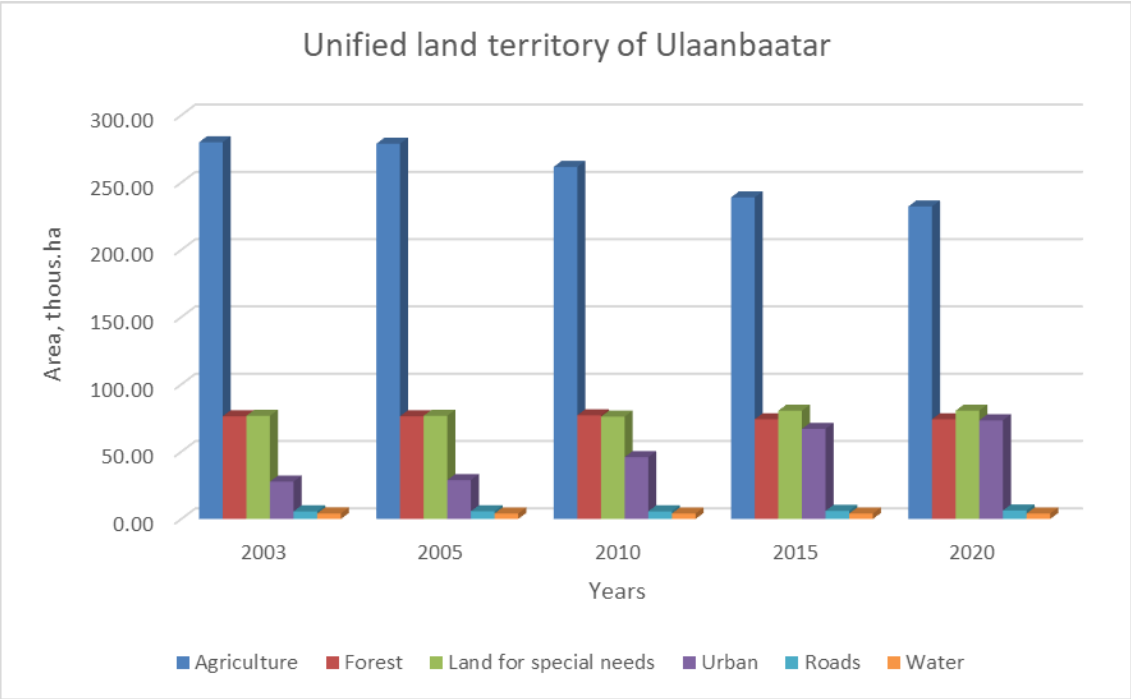

Figure 4. Land-use changes in Ulaanbaatar

Several studies have been conducted to determine the impact of land use and climate changes on the Tuul river quality based on field studies or laboratory experiments (8), (9). Naturally, river water is capable of purifying itself as a river flows downstream [65]. However, the results of research in the field of land-use changes (10) showed that the Tuul river is no longer able to purify itself completely until flowing into the Orkhon river. Moreover, in determining the physical and chemical properties of the water of the Tuul river and its tributaries in 2015 (11), the values such as biochemical oxygen demand 155.1 mg/L at downstream of Tuul-Songino sampling point, 48.9 mg/L at Tuul-Khadan-Khysaa and, 5.4mg/L at Tuul-Shine-Guur, ammonium ions 1.23 mg/L – 12.77 mg/L, phosphate ions 0.1 mg/L – 0.7 mg/L, Pb 9.1 mg/L and Zn 91.3 mg/L were measured and significantly exceeded a corresponding MNS 4686-98 standard. Due to poor operation of Central Wastewater Treatment Plant, downstream of Tuul-Songino, Tuul-Khadan-Khysaa, Tuul-Shine-Guur sampling points are highly polluted or are categorized as 6^{th} pollution level according to the surface water quality index (11). Addition to this, in the Tuul River Basin, the average annual temperature around Ulaanbaatar has increased by 2.6°C over the last 75 years, and precipitation has decreased by 5 percent due to the expansion of urban land use (12).

The quality of the Tuul river and its tributaries has been determined mainly based on the surface water quality index, which is calculated by performing laboratory analysis on collected water samples from various sampling points along the Tuul river. However, there is a lack of studies to assess the impact of land-use change on streamflow and quality through the application of surface water modeling. Therefore, there is a need to study and evaluate the impacts of land use and climate changes on the Tuul river basin. One of the best practices to quantify streamflow and analyze water quality is the application of a hydrological model with a spatial and point scale. Soil and Water Assessment Tool (SWAT) is a river basin model which can simulate changes in the hydrologic response, water quality, and erosion of a watershed, as well as evaluating the effects of land-use changes and climate variability on a river basin over short and long periods of time (13). Therefore, this study used SWAT surface water modeling to evaluate the effects of land-use changes on surface water quantity and quality in the upper part of the Tuul river basin.

1.1 Objectives

The main objective of this study is to assess the impact of land use changes on surface water quality and quantity of the upper part of the Tuul river subbasin using the SWAT hydrological model with the following specific objectives:

- To prepare input data for SWAT model (e.g., spatial and weather data)
- To calibrate and validate the ArcSWAT model in the study area
- To analyze the land-use effects on Tuul river surface water quantity and quality

2. State of the art

2.1 Literature review on modeling application

Land-use and land cover (LULC) changes, for example, a transformation from pasture land or forest area to urban and residential area due to the rapid growth of population and urbanization, have an adverse impact on water balance (14). These changes may lead to an increase or decrease in regional hydrological components such as evapotranspiration (ET), soil moisture, and surface runoff (15). Moreover, water quality can also be affected by human-induced ecosystem changes. Therefore, studying the consequences of LULC changes is important for the preservation of water resources and planning urbanization (16). The SWAT model is used widely in various regions of the world to predict the impacts of LULC and climate changes on complex watersheds as well as to simulate both surface and groundwater quality and flow (17). The following studies used the SWAT model in their study area owing to its reliability, efficiency, and wide application as a watershed modeling tool to evaluate hydrological processes. These studies differ from each other by parameters' sensitivity and calibration due to the location of the study areas, climate conditions, dominant land use types, and availability of input data needed for the model simulation. Impact of LULC change on streamflow and water quality varies differently depending on predominated land use types. For instance:

The studies (18), (19), (20), (21) applied the SWAT model in the watersheds of their study areas, which are predominated by agricultural lands, to determine the effect of land-use changes on discharge, sediment transport, and discharging of inorganic compounds. The results of the model regarding land-use changes showed that an increase in agricultural land-use leads to an increase in discharge, surface runoff, total suspended solid, total nitrogen and total phosphorus. For the reason that agricultural land deteriorates soil significantly and high amount of fertilizer is used in this field.

Moreover, SWAT model was used to simulate the effects of land cover changes due to coal mining activities on discharge and sediment yield (22). Changes in LULC and soil characteristics in the watershed by mining activities caused a decrease in percolation, lateral flow, and groundwater, as well as an increase in surface runoff. Furthermore, another research (14) studied the effect of abandoned mining on hydrology. This analysis differed from previous studies which were conducted in mining-dominated river basins by the simulation results of the SWAT model. The abandoned open-pit mining altered the hydrological components with an increase in sediment yield, groundwater flow,

evapotranspiration, and a decrease in surface runoff. Many potholes were left after mining activities stopped. Therefore, generated runoff in this watershed is gathered in these potholes instead of flowing into the streams.

Furthermore, one of the major land-use changes affecting hydrologic processes could be an expansion of forest area. The SWAT model was used to evaluate LULC changes on hydrological components in afforested river basin (23). As the amount of forest area grows, so does the rate of infiltration and transpiration, resulting in a rise in base flow and evapotranspiration. On the other hand, surface runoff and water yield decreased. Also, this study modeled the impacts of extreme LULC scenarios, for example conversion from all agricultural land to forest or from grassland to forest area, on hydrology. Because of the high evapotranspiration from the expansion of forest areas in these scenarios, the basin would be more vulnerable to water stress.

According to the study (24), intermediate and high-density residential development can support reducing excess total suspended solid (TSS) levels, whereas dense commercial and industrial growth can help mitigate high phosphorus levels. In addition to this, the influence of LULC modification contributes to an increase in streamflow and a decrease in evapotranspiration because of increased urbanization and decreased water bodies and forest area (25).

The above-mentioned studies concluded that the SWAT hydrological model acts as a robust model for simulating hydrological components at different land use and climate regimes.

2.2 Model application in Mongolia

In recent years, research has been conducted to assess surface water resources and its regimes in Mongolian river basins using different types of surface water models such as TOPLATS and HEC-HMS (26), (27). On the other hand, only a few modeling studies applying SWAT model have been conducted in the Tuul river basin; in one study, the ArcSWAT model was used to simulate nutrient loads and discharge in an upper part of the Tuul river basin (28). The SWAT model was also used to model watershed hydrologic processes and their influence on water resources throughout the Tuul river basin (29). These studies concluded that the SWAT model was relatively good at estimating streamflow and that simulation of the model satisfactorily captures the watershed's hydrological processes. Nevertheless, no studies have been investigated to assess the impact of land-use changes on both water quantity and quality model in the Tuul river basin using the ArcSWAT model.

2.3 Overview of SWAT model

2.3.1 Introduction

The Soil and Water Assessment Tool is a well-known river basin-scale model which was originated from the United States Department of Agriculture and Agricultural Research Service (USDA-ARS) (17). It is a continuous-time model that works on a daily time step that's usually used to estimate the impact of land management strategies on water, and sediment yields in enormous complex watersheds with altering soils, land use, and management circumstances over long periods of time (30). The model is based on the laws of physics with natural processes, is computationally useful and efficient, and has the ability to develop long-term simulations. Weather, soil surface temperature, its characteristics, hydrology, plant growth, pesticides, bacteria and pathogens, nutrients, and land-use patterns are all crucial components of the model. The model is widely used to determine surface flow and assess the impacts of land-use and land management processes, climate change, and to examine water quality within river basins or subbasins.

2.3.2 Evolution of model

The first version of the ArcSWAT model was created in the early 1990s as version 94.2. The USDA-ARS conducted over 30 years of modeling experiments and research that led to the development of the SWAT model, and the current version of SWAT incorporates the general concepts of USDA-ARS and other models. Pesticide transport, hydrological, and crop growth models are derived from the USDA-ARS small basin-level models including GLEAMS (groundwater loading effects of agricultural management system) (31), CREAMS (chemical, runoff and erosion from agricultural management systems) (32), EPIC (erosion-productivity impact calculator) (33). The SWRRB model (simulator for water resources in rural basins) is used first, which comprises sub-models like a meteorological data producing database, sediment movement orientation, and surface and groundwater sub-models.

The first version of the ArcSWAT model was integrated with the ROTO (Routing outputs to outlet) model to determine the direction and structure of channel and reservoir routing to work with the SWRRB sub-model. The QUAL2E model allows determining the instream kinetic routine and the sediment transport routine at the level of reservoirs, ponds, wetlands, and septic tanks (34).

2.3.3 Model components

In the SWAT model, a basin is divided into several subbasins in the watershed delineation process, and subbasins are further partitioned into the hydrologic response units (HRUs) (35). When different land-use types are dominated throughout a basin, using subbasins in a simulation is beneficial (36). In SWAT simulation, the hydrologic cycle of a basin can be separated into two major parts; the land phase (upland processes), and the routing phase (channel processes). The land phase controls the amount of water, sediment, and nutrients that flow into each subbasin's main channel. The movement of water, sediments, and other materials through the watershed's channel network to the outlet is defined by channel processes (30). During the land phase processes, the hydrologic cycle is calculated based on the water balance equation.

$$SW_t = SW_0 + \sum_{i=1}^{t} (R_{day} - Q_{surf} - E_a - w_{seep} - Q_{gw})$$

where SWt: the final soil water content (mm H_2O)

SW_0: the initial soil water content on day i (mm H_2O)

t: the time (days)

R_{day}: the amount of precipitation on day i (mm H_2O)

Q_{surf}: the amount of surface runoff on day i (mm H_2O)

E_a: the amount of evapotranspiration on day i (mm H_2O)

w_{seep}: the amount of water entering the vadose zone from the soil profile on day i (mm H_2O)

Q_{gw}: the amount of return flow on day i (mm H_2O) (30).

As the water cycle in nature takes place under the influence of climatic factors, inputs from moisture, and energy sources are necessary. These include precipitation, maximum and minimum temperature values, solar radiation, wind speed, and relative humidity. These variables control the water cycle in nature.

The ArcSWAT model reads directly from the above-mentioned daily observed meteorological data to calculate the water movement in HRUs. SWAT models the following hydrological components including infiltration, surface runoff, canopy storage, lateral flow, return flow, potential evapotranspiration, and actual evapotranspiration (Figure 5).

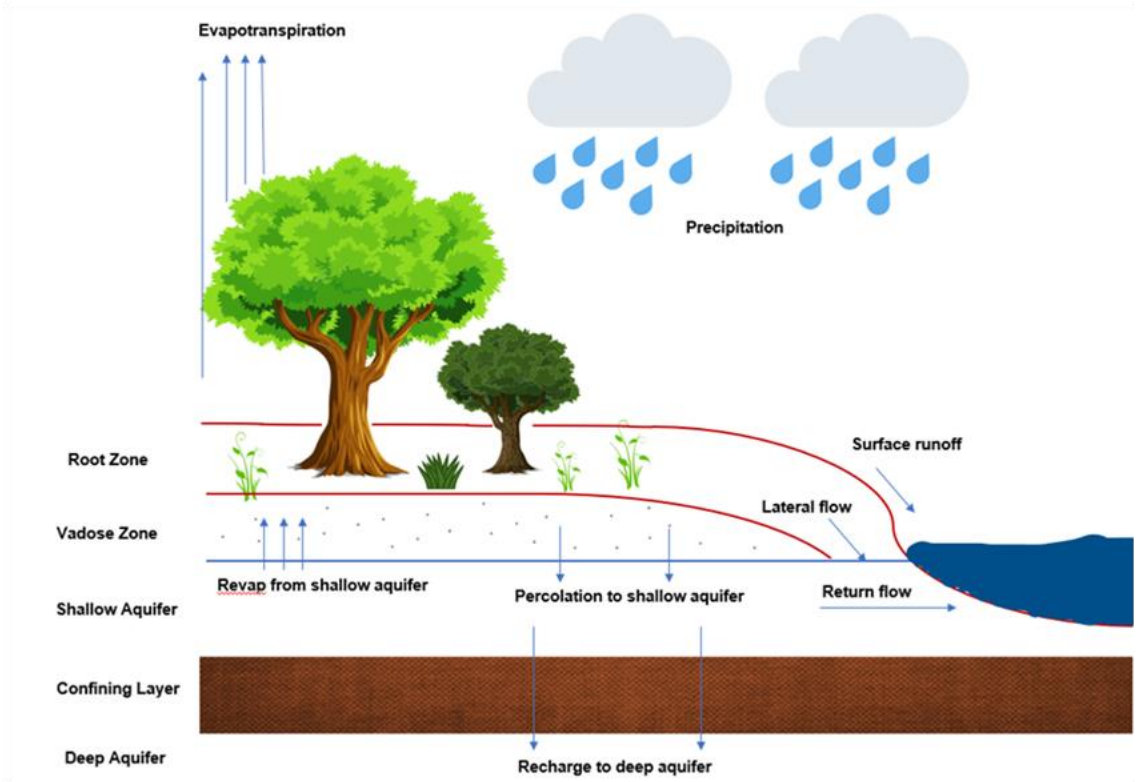

Figure 5. Hydrologic cycle simulated in SWAT (30)

Surface runoff. Surface runoff is an overland flow that occurs when the rate of water falling into the ground surface exceeds the infiltration rate. A dry soil has a high infiltration rate. However, when the soil begins to saturate with moisture, the infiltration rate decreases. The SWAT model uses two methods, the SCS curve number method (36) and Green & Ampt infiltration method (37), (38) to calculate surface runoff. The SCS curve number method was used in this study. The SCS equation (30) is:

$$Q_{surf} = \frac{(R_{day} - I_a)^2}{(R_{day} - I_a + S)} \qquad (1)$$

Q_{surf} – Accumulated runoff, mm

R_{day} – Rainfall depth of the day, mm

I_a- Initial abstraction, mm

S- Retention parameter, mm

The initial abstraction value depends on surface water storage capacity and infiltration, while the retention parameters indicate different surface slopes, soil cover, and different land-use types. The retention parameter (30) is calculated by the equation:

$$S = 25.4\left(\frac{1000}{CN} - 10\right)$$

CN: Curve number for the day

Generally, the initial abstraction I_a is estimated as 0.2S, thus the equation (1) can be rearranged as:

$$Q_{surf} = \frac{(R_{day} - 0.2S)^2}{(R_{day} + 0.8S)}$$

The typical curve numbers for different land cover and soil types are shown in Table 1, and Table 2. Based on the capability of infiltration of the soils under different land cover conditions, soils are classified into four hydrologic groups (30). The hydrologic soil groups are A: low runoff potential; B: moderate infiltration rate; C: slow infiltration rate; and D: high runoff potential.

Table 1. Other agricultural land-Runoff curve number

Cover		Soil group			
Cover type	Hydrologic condition	A	B	C	D
Pasture, grassland, and range – continuous grazing for livestock	Poor	68	79	86	89
	Fair	49	69	79	84
	Good	30	61	74	80
Meadow-continuous grass that is cultivated for hay and is protected from grazing	----	30	58	71	78
Brush-brush weed-grass mix with the brush as the primary component	Poor	48	67	77	83
	Fair	35	56	70	77
	Good	30	48	65	73
Combination of wood and grass	Poor	57	73	82	86
	Fair	43	65	76	82
	Good	32	58	72	79

Woods	Poor	45	66	77	83
	Fair	36	60	73	79
	Good	30	55	70	77
Farmsteads-buildings, roadways, and driveways	----	59	74	82	86

Table 2. Urban area-Runoff curve number

Cover		Soil group			
Cover type	Hydrologic condition	A	B	C	D
Openspaces, cemeteries, lawns and parks, etc.	Poor	68	79	86	89
	Fair	49	69	79	84
	Good	39	61	74	80
(Impervious area)					
Parking lots (paved), driveways, roofs, etc.	----	98	98	98	98
Streets and roads (paved), open ditches, etc.	----	83	89	92	93
Gravel streets and roads	----	76	85	89	91
Dirt streets and roads	----	72	82	87	89

Potential and actual evapotranspiration. There are several methods for calculating potential evapotranspiration. The SWAT model offers the Penman-Monteith method (39), (40), (41), the Priestley-Taylor method (42), and the Hargreaves method (43). These three methods require different input data. When the Priestley-Taylor method is used, input data such as solar radiation, air temperature, and relative humidity are required while the Penman-Monteith method requires solar radiation, air temperature, relative humidity, and wind speed. On the other hand, the Hargreaves method requires only air temperature (30). Since all the required input data for the Penman-Monteith method are available in the study area, the potential evapotranspiration was estimated by this method. The following equation and Table 3 describe the calculation of Penman-Monteith method.

$$\lambda E_t = \frac{\Delta(H_{net} - G) + \gamma * K_1 * (0.622 * \lambda * p_{air}/P) * (e_z^0 - e_z)/r_a}{\Delta + \gamma * (1 + \frac{r_c}{r_a})}$$

Table 3. Penman-Monteith method (30)

	Parameters	Description	Unit	Equation
1	H_{net}	Net radiation	MJ/m^2*day	
2	γ	Psychometric constant	kPa/^{0}C	$\Upsilon = \frac{c_p * P}{0.622 * \lambda}$ $P = 101.3 - 0.1152EL + 0.544 * 10^{-6} * EL^2$
3	λ	Latent heat vaporization	MJ/kg	$\lambda = 2.501 - 2.361 * 10^{-3} * T_{av}$
4	e_z	Water vapor pressure of air at height z	kPa	$= exp\left[\frac{16.78 * T_{av} - 116.9}{T_{av} + 237.3}\right]$
5	e_z^0	Saturation vapor pressure of air at height z	kPa	$= R_h * e_z$
6	Δ	Slope of the saturation vapor pressure-temperature curve	kPa/^{0}C	$\Delta = \frac{4098 * e_z}{(T_{av} + 237.3)^2}$
8	K_1	Dimension coefficient	m/s	= 8.64*10^4
9	P	Atmospheric pressure	kPa	$P = 101.3 - 0.1152EL + 0.544 * 10^{-6} * EL^2$
11	r_a	Diffusion resistance of the air layer	s/m	$= \frac{114}{u_z}$
12	r_c	Plant canopy resistance	s/m	$LAI = 1.5 * ln(h_c) - 1.4 = 4.1$ $r_c = 49/\left(1.4 - 0.4 * \frac{CO_2}{330}\right)$

After the calculation of potential evapotranspiration, actual evapotranspiration was determined using a similar method that is suggested by Richtie (44).

3. Materials and method

3.1 Study Area

The Tuul river is one of the longest rivers of Mongolian surface water resources. The river originates from the Chisaalai Saridag and Shorootyn Davaa at an altitude of 2289.2 meters and flows into the Orkhon River. The elevation of the river basin ranges from 770 to 2800 meters, and most of the tributaries originate from the Baga Khentii mountain (8). The Tuul river initially flows through the mountain taiga and forest-steppe regions, then through the steppe regions below Ulaanbaatar. The Tuul river basin is 717 km long and has a total catchment area of 49774.3 km^2, covering 37 soums of five provinces (Arkhangai, Bulgan, Selenge, Uvurkhangai, and Tuv) and 7 districts of Ulaanbaatar city. It is surrounded by mountains elevated above sea level; thus, there is a great difference in day and night temperatures; the winter season is longer than the summer season, and the precipitation falls mainly during the rainy season (June to September). Annual average precipitation varies from 252.9-275 mm in the river basin (45). Groundwater accounts for 25 percent of the Tuul river's streamflow; 6 percent for snowmelt, and 69 percent for spring, summer, and autumn rainfall (8), (46). According to stream gauging station's observed data between 2008 and 2019, the mean annual streamflow near a Tuul-Altanbulag gauging station was 10.1 m^3/s. The study area is found from the origin of the Tuul river basin to the outlet point at the Tuul-Altanbulag gauging station (Figure 6). The upper part of the study area is dominated by forest areas and continues into a lower part with residential, industrial and pasture land areas.

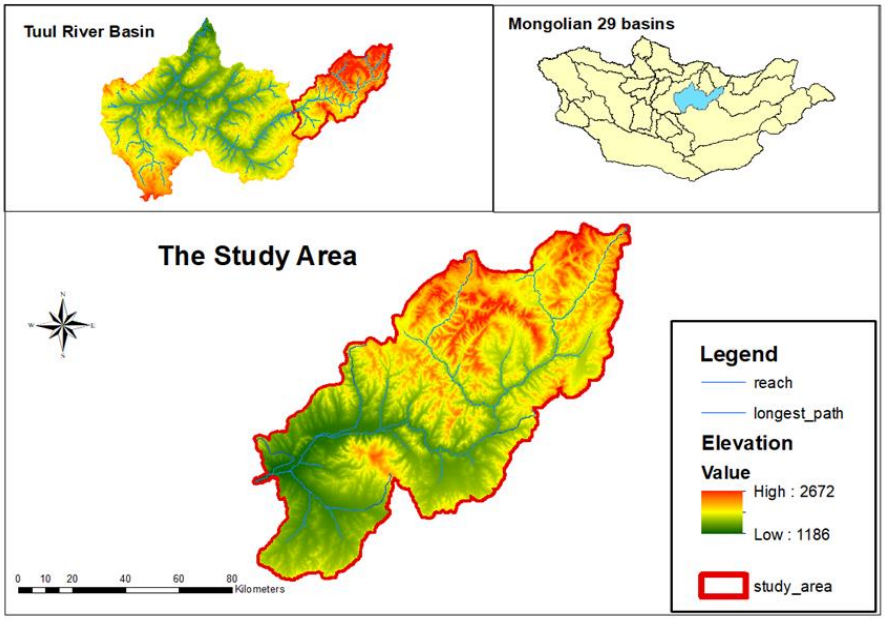

Figure 6. The study area map

3.2 SWAT input data

Spatial data (DEM, land use, land cover, topography, soil map) and meteorological data (precipitation, air temperature, relative humidity, wind speed, and solar radiation) are required as input data to run SWAT model. Table 4 provides the data types and their sources used in the study.

Table 4. Data sources

Data	**Period**	**Data source**
Meteorological data		
Precipitation	2008-2019	The National Agency for Meteorology, Hydrology and the Environmental monitoring (NAMHEM)
Air temperature	2008-2019	
Relative humidity	2008-2019	
Wind speed	2008-2019	
Solar radiation	2008-2019	
Spatial data		
Land use, land cover	2010, 2015, 2019	Landsat images from United States Geological Survey USGS
Digital Elevation Model (DEM)		
Soil		Harmonized World Soil Database from FAO
Water catchment area, Surface water network		The Tuul river basin
Observed data		
Discharge	2008-2019	NAMHEM
Water quality	2019	

3.2.1 Spatial data

DEM: The ArcSWAT model automatically delineates subbasins based on the Digital Elevation Model (DEM). Mapping subbasins requires the use of DEM in ESRI grid format. DEM with 90m x 90m resolution was used in the watershed delineation of the study area and the Tuul-Altanbulag (latitude: 47.69°, longitude: 106.41°) and Tuul-Ulaanbaatar (latitude: 47.92°, longitude: 106.85°) gauging stations were used as sub-basin outlet points.

LULC data: Landsat satellite images for July 2010 (Landsat-5 TM), August 2015 (Landsat-8 OLI), and August 2019 (Landsat-8 OLI) were downloaded from United States Geological Survey (USGS) online site. Radiometric and atmospheric corrections were already performed for these satellite images by the USGS EROS Digital Image Processing Center (47). After extracting the region of interest from satellite images, land use and land cover maps for 2010, 2015, and 2019 were prepared using the maximum likelihood supervised classification method with ArcGIS software (48). During the supervised classification, LULC classes were classified in the study area based on eighteen classes of LULC which are defined in the SWAT database (Table 5).

Table 5. Main 18 land use types in SWAT database

	Name	Code	Representative plant	Plant type
1	Agricultural land-generic	AGRL	Grain sorghum	Warm season annual
2	Agricultural land-row crops	AGRR	Corn	Warm season annual
3	Agricultural land-close grown	AGRC	Winter wheat	Cool season annual
4	Orchard	ORCD	Apples	Trees
5	Hay	HAY	Oak	Perennial
6	Forest-mixed	FRST	Oak	Trees
7	Forest-deciduous	FRSD	Oak	Trees
8	Forest-evergreen	FRSE	Pine	Trees
9	Wetlands	WETL	-	Perennial
10	Wetlands-forested	WETF	Oak	Trees
11	Wetlands-nonforested	WETN	Oak	Perennial
12	Pasture	PAST	Oak	Perennial
13	Summer pasture	SPAS	Oat	Perennial
14	Winter pasture	WPAS	-	Perennial

15	Range-grasses	RNGE	-	Perennial
16	Range-brush	RNGB	-	Perennial
17	Residential area	URBN	-	-
18	Water	WATR	-	-

Soil data: Soil data required for the model were prepared from the FAO International Soil Classification Map and the MWSWAT database. The FAO Soil Classification Map categorizes a total of 106 soil classifications worldwide, and the following 16 soil types are identified in the study area (Table 6).

Table 6. Soil classifications based on FAO in the study area

	FAO soil code	**FAO soil name**	**Area, km^2**	**Area, %**
1	I-Bh-U-C-3098	Gelic Umbrisols	2133.28	23.92
2	I-Mo-2c-4385	Colluvic Cryosols	291.94	3.27
3	I-Dd-Rd-2-3973	Gelic Phaoezems	684.50	7.67
4	Ch19-3a-4314	Leptic Histic Cryosols	47.43	0.53
5	Kh1-2ab-3159	Relicitigleyic Kastanozems	873.51	9.79
6	I-Bh-U-2c-3096	Umbrisols	1363.18	15.28
7	Cg4-3a-4310	Non calcic Chernozems	151.91	1.7
8	I-Mo-2c-3116	Fluvisols	53.81	0.6
9	Cg4-3a-4309	Non-Calcic Chernozems	51.05	0.57
10	Kh1-2b-4232	Kastanozems	1380.97	15.48
11	I-Bh-U-C-3968	Mollic Umbrisols	515.88	5.78
12	Ch19-3a-4313	Chernozems	931.44	10.44
13	I-Dd-Rd-2-4220	Cryic Phaoezems	48.17	0.54
14	Kh1-2b-3994	Kastanozems	181.80	2.04
15	I-K-2c-3974	Leptic Kastanozems	151.14	1.69
16	I-Mo-2bc-3115	Salic Phaeozems	59.55	0.67

3.2.2 Meteorological data

Weather input data for the SWAT model should include daily measured data of precipitation (mm), air temperature (°C), relative humidity (fraction), solar radiation (MJ/m^2), and wind speed (m/s). Those weather data were obtained from the National Agency for Meteorology, Hydrology and the Environmental Monitoring for the period 2004 to 2019. Daily observation data (maximum and minimum air temperature, precipitation, wind speed, relative humidity, solar radiation) from Ulaanbaatar, Terelj, and Buyant-Uhaa weather stations were prepared in the format of SWAT weather input data. Locations of weather stations and stream gauges are shown in Figure 7.

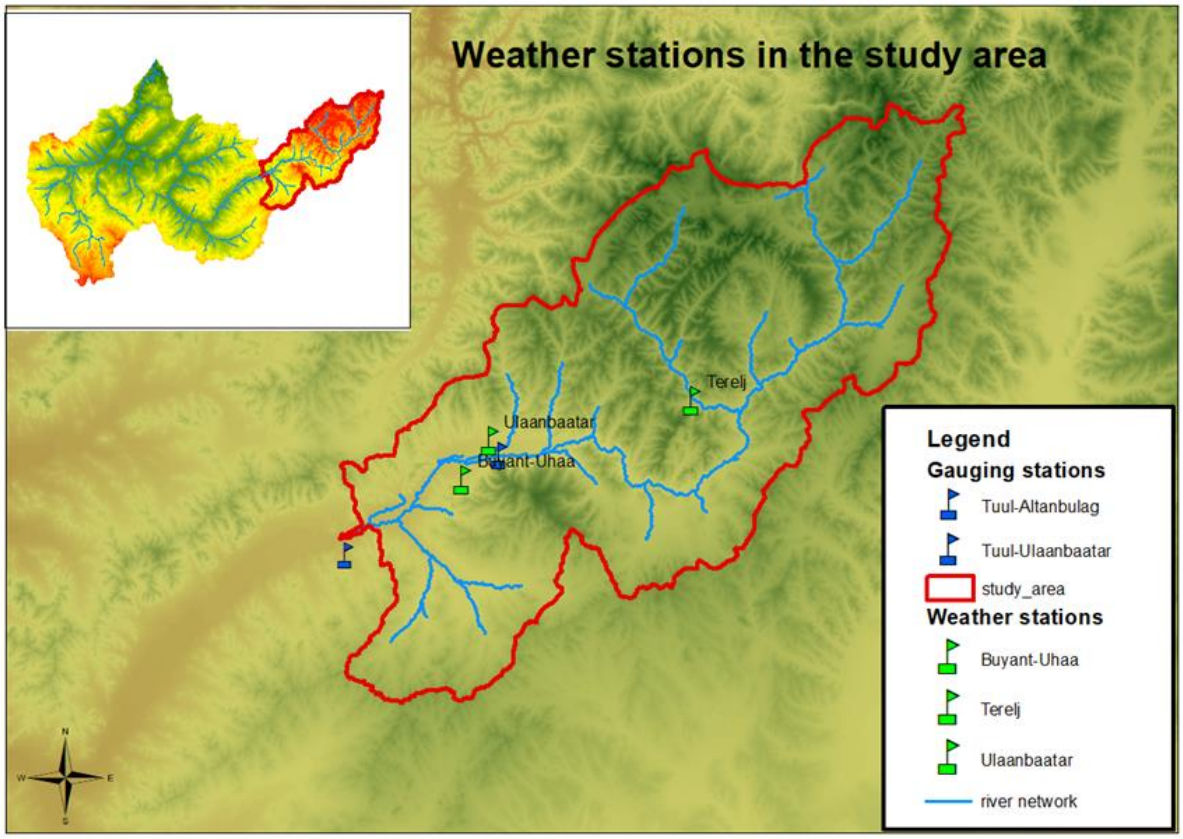

Figure 7. Location of weather stations

3.3 Model sensitivity analysis, Calibration, Validation

The SWAT model was calibrated with the SWAT-CUP (SWAT-Calibration and Uncertainty Programs) which is a program developed for auto-calibration, sensitivity analysis, and validation of the SWAT model's results (49), (50), (51), (52). Several uncertainty algorithms are available for the application of SWAT-CUP autocalibration including Generalized Likelihood Uncertainty Estimation "GLUE" (53), Solution parameters "Parasol" (54), and Sequential Uncertainty Fitting "SUFI-2" (55), (56). The SUFI-2 algorithm was used for model sensitivity and uncertainty analysis, calibration and validation.

3.3.1 Uncertainty analysis

In the SUFI-2, the p-factor and r-factor are calculated to determine the strength of the calibration and the model's uncertainty. The p-factor is the fraction of observed data that is covered by the 95 percent prediction uncertainty (PPU) and the average distance $\bar{d}$ between the upper and the lower 95PPU, which is calculated from:

$$\bar{d}_x = \frac{1}{k}\sum_{l=1}^{k}(X_U - X_L)_l$$

Where k is the number of observed data points, the 2.5th (X_L) and 97.5th (X_U) percentiles represent the lower and upper boundaries of the 95PPU (55). The R-factor is the ratio of the 95PPU band's average width to the measured variable's standard deviation. That is calculated by:

$$R - factor = \frac{\bar{d}_X}{\sigma_X}$$

Where σ_X is the standard deviation of the measured variable X. Generally, the p-factor and r-factor get smaller as parameter ranges decrease (49).

3.3.2 Sensitivity analysis

The most important step in the calibration and validation process of SWAT-CUP is sensitivity analysis, which defines the most sensitive parameters for a study area (57). There are two types of sensitivity analysis (one-at-a-time and global sensitivity). One-at-a-time sensitivity analysis is conducted by changing each parameter ‘s value individually while maintaining constant values of other parameters. On the other hand, all parameters are changing at the same time in the global sensitivity (57). The SWAT-CUP uses statistical measurements t-stats and p-values to identify the sensitive parameters. Larger t-stats and p-values close to zero indicate greater sensitivity (49).

3.3.3 Calibration and Validation

Model calibration means adjusting the optimal values of input parameters by comparing model simulation results with observed data for a given watershed. After calibration, the model is validated with input parameters determined during calibration. The validation process is performed for a different period of observed data which is not used in the calibration process (58). The purpose of validation is to prove the model’s performance (59). Nash-Sutcliffe efficiency coefficient (NSE), the correlation coefficient (*r*), and percentage bias (PBIAS) were used to evaluate the performance of SWAT model

outputs. The NSE is a measure of how closely the observed versus simulated data plot fits the 1:1 line (60).

$$NSE = 1 - \left[\frac{\sum_{i=1}^{n}\left(Y_i^{observed} - Y_i^{simulated}\right)^2}{\sum_{i=1}^{n}\left(Y_i^{observed} - Y_i^{mean\ of\ observed}\right)^2}\right]$$

PBIAS evaluates whether a simulated value is greater or less than the observation. A positive PBIAS value indicates underestimation and a negative value refers to overestimation (61).

$$PBIAS = 100 * \frac{\sum(Y^{observed} - Y^{simulated})_i}{\sum(Y_i^{observed})}$$

4. Result and discussion

The input data required for the ArcSWAT modeling including daily air temperature (°C), precipitation (mm), wind speed (m/s), relative humidity, and solar radiation from 2004 to 2019 was prepared. Additionally, following spatial data was produced within the framework of the study area.

The ArcSWAT model used DEM to delineate subbasins in the study area. River basin delineation was performed using the location of the Tuul-Ulaanbaatar and Tuul-Altanbulag gauging stations. From the result of the SWAT watershed delineator, the upper part of the Tuul-Altanbulag gauging station was divided into six subbasins (Figure 8), and the study area has a total of 8919.6 km^2 area. Determining surface water resources by ArcSWAT modeling requires the Hydrologic Response Units (HRUs) to be calculated based on the homogeneous land use, soil and surface slope classifications within sub-basins (Figure 9) (30). Therefore, LULC, soil, and surface slopes were classified.

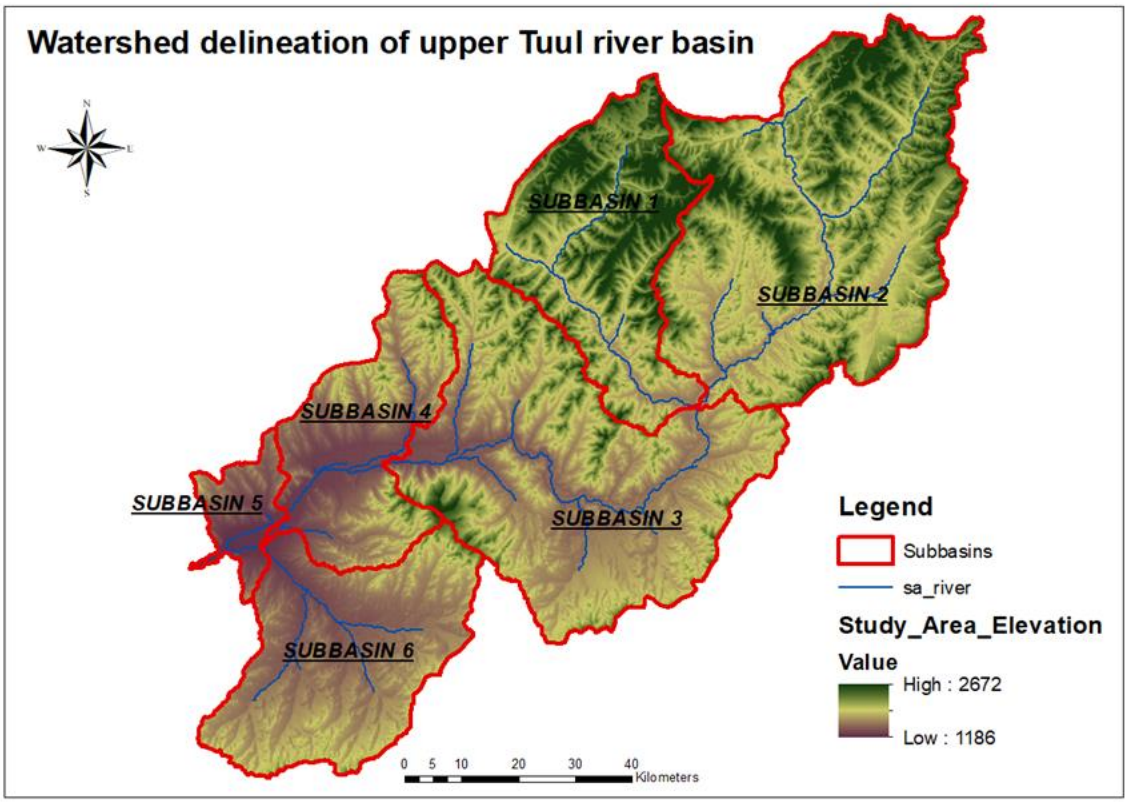

Figure 8. Watershed delineation

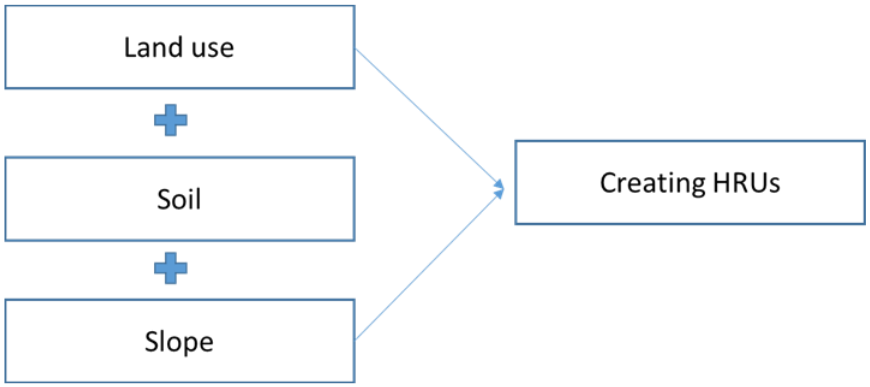

Figure 9. HRUs calculation

Land use, land cover classification. The LULC maps for 2010, 2015 and 2019 were classified using the maximum likelihood supervised classification method with ArcGIS software. The LULC maps were categorized into the main four LULC types: Water body, Urban, Pasture, and Forest (Figure 10).

a)

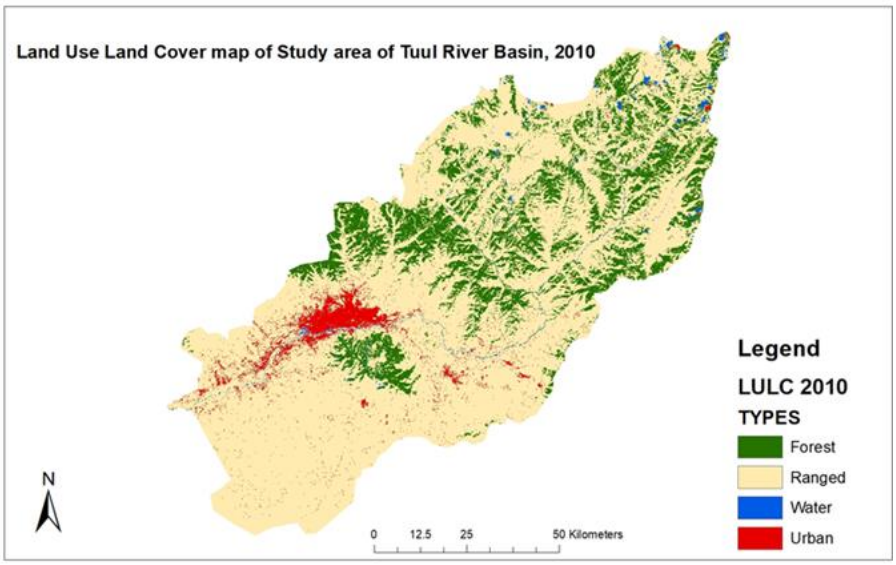

b)

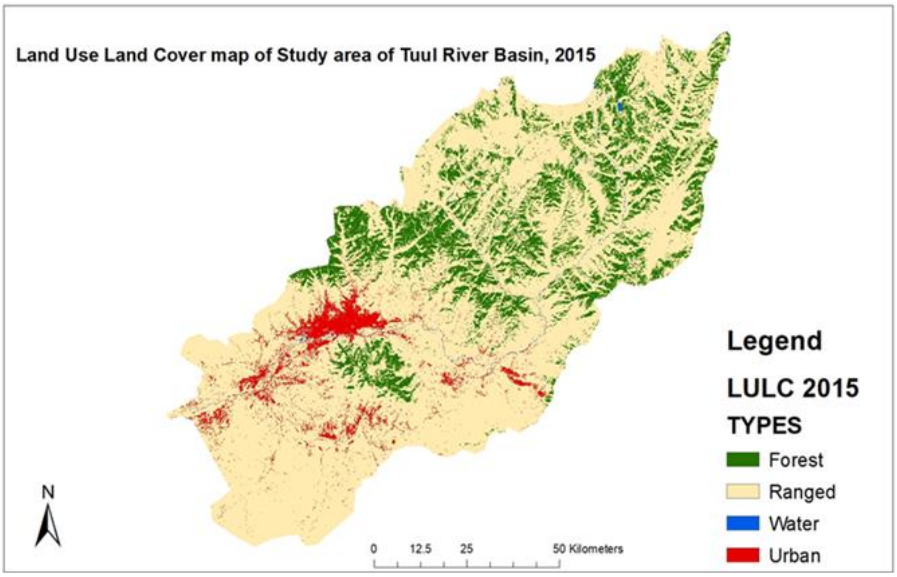

c)

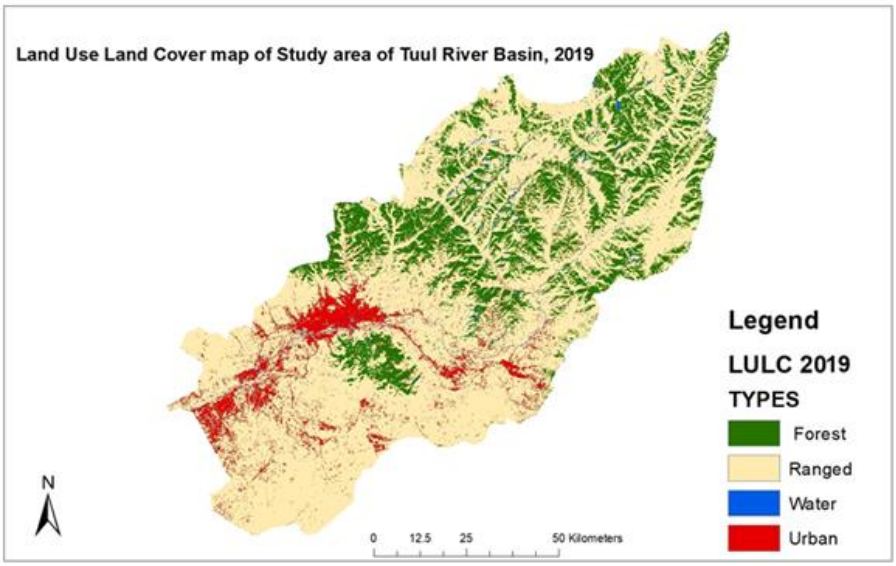

Figure 10. LULC maps (a) in 2010 (b) in 2015 (c) in 2019

The LULC classifications showed that the forest area in 2019 was increased by about 2%; the pasture area was decreased by 5%, and the urban area was expanded by 3% compared to the LULC map in 2010 (Table 7).

Table 7. The area of the LULC classifications

LULC types	**2010**		**2015**		**2019**	
	Area (km^2)	Area (%)	Area (km^2)	Area (%)	Area (km^2)	Area (%)
Forest	1790.96	20.08	1680.51	18.84	1965.25	22.03
Ranged	6768.66	75.89	6820.11	76.46	6309.47	70.74
Urban	290.86	3.26	387.98	4.35	561.18	6.29
Water	69.1	0.77	30.97	0.35	83.68	0.94
Total	8919.57	100.00	8919.57	100.00	8919.57	100.00

Accuracy assessment of LULC classification. Kappa coefficient were used to validate predicted LULC classifications. Kappa is the most effective method used to measure accuracy between classified images and reality (62), (63). To maintain spatial randomness and distribute points proportionately throughout land cover classes, stratified random sampling was used (64). A total of 400 random reference points were generated within the study area and the correctness of each random point was validated from Google Earth Image (Figure 11).

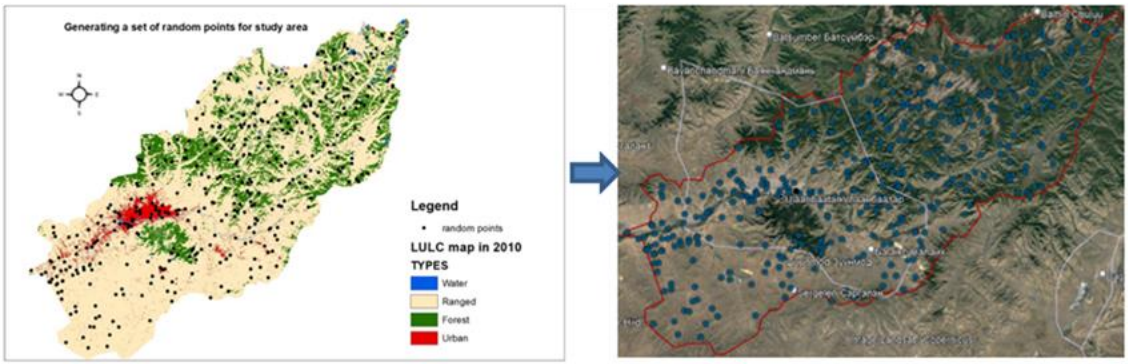

Figure 11. Validating generated random points in ArcMap with Google Earth

The overall accuracy and kappa coefficients of classified images were 0.74, 0.76, 0.64, and 80.25%, 82.3%, and 73.25% for the years 2010, 2015, and 2019, respectively (Table 8). According to the level of agreement of kappa values (62), (65), classified images have substantial agreement with the trusted source Google Earth map (Table 9).

Table 8. Accuracy assessment of 2010, 2015, 2019 maps

	Types	Forest	Ranged	Urban	Water	Row total	UA (%)
2010	Forest	**94**	6	0	0	100	94
	Ranged	1	**95**	3	1	100	95
	Urban	1	14	**85**	0	100	85
	Water	27	26	0	**47**	100	47
	Column total	123	141	88	48	**400**	
	PA (%)	76.42	67.38	96.59	97.92		
	OA = 80.25%; **K=0.74**						
	Types	Forest	Ranged	Urban	Water	Row total	UA (%)
2015	Forest	**98**	2	0	0	100	98.00
	Ranged	4	**92**	4	0	100	92.00
	Urban	0	24	**72**	4	100	72.00
	Water	21	12	0	**67**	100	67.00
	Column total	123	130	76	71	**400**	
	PA (%)	79.67	70.77	94.74	94.37		
	OA = 82.3%; **K = 0.76**						
	Types	Forest	Ranged	Urban	Water	Row total	UA (%)
2019	Forest	**100**	0	0	0	100	100
	Ranged	2	**94**	3	1	100	94
	Urban	6	25	**69**	0	100	69
	Water	25	43	2	**30**	100	30
	Column total	133	162	74	31	**400**	
	PA (%)	75.19	58.02	93.24	96.77		
	OA = 73.25%; **K=0.64**						

OA: Overall accuracy; K: Kappa coefficient; UA: User's accuracy; PA: Producer's accuracy

Table 9. Level of agreement of Kappa values

Values	Strength of Agreement
<0	Poor
0.01-0.4	Slight
0.41-0.6	Moderate
0.61-0.8	Substantial
0.81-1	Almost perfect

Soil classification. The FAO International Soil Classification Map and the MWSWAT database were used to create the soil data for the SWAT model. The FAO Soil Classification Map categorizes a total of 106 soil categories around the world, of which 16 are found in the research region (Figure 12). After re-classification, the land use, soil, and slope below threshold levels are not considered in the subbasins (66). The soil types after re-classification in the ArcSWAT model can be shown in Table 10.

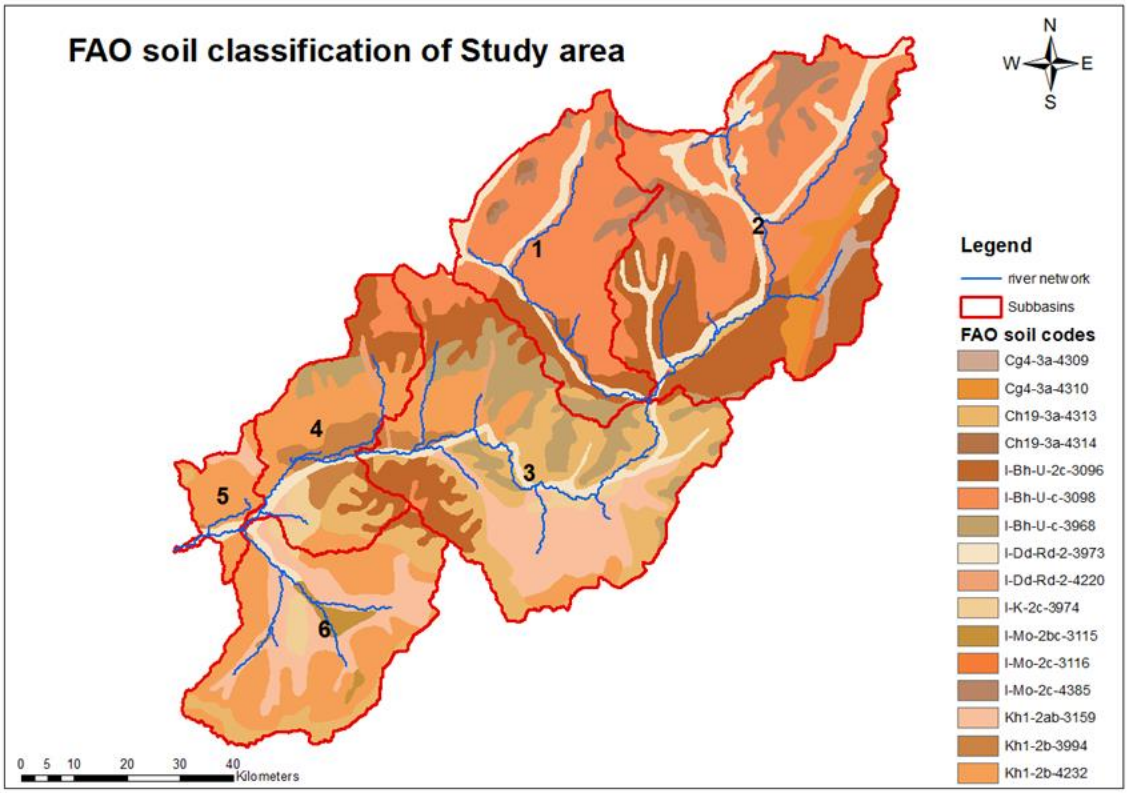

Figure 12. Soil classification in the study area

Table 10. Soil data after reclassification in the model

Soil code	Area (km^2)	Area (%)	Rooting depth (mm)
I-Bh-U-c-3098	302.7	28.52	460
I-Dd-Rd-2-3973	144.7	6.4	690
I-Bh-U-2c-3096	10.2	15.39	460
I-Bh-U-c-3968	44.2	6.32	460
Ch19-3a-4313	81.9	12.32	1000
Kh1-2ab-3159	103.6	11.39	1000
Kh1-2b-4232	215.7	18.72	880
Kh1-2b-3994	18.4	0.93	300

Table 11. Curve numbers based on soil and land use types in the study area

Soil types	Hydrologic soil group	URBN	FRST	RNGE
		Urban area	Forest	Pasture, grassland
I-Bh-U-c-3098	C	-	73	79
I-Dd-Rd-2-3973	C	72	73	79
I-Bh-U-2c-3096	C	-	73	79
I-Bh-U-c-3968	C	-	73	79
Ch19-3a-4313	C	-	73	79
Kh1-2ab-3159	C	72	-	79
Kh1-2b-4232	C	72	-	79
Kh1-2b-3994	C	72	-	-

Slope classification and HRUs definition. The surface slope was divided into four classes (Table 12) with a five percent increment using DEM (30). The threshold level of LULC/Soil/Slope: 5%/10%/10% was applied in the HRU definition part of the SWAT model which resulted in the further division of sub-basins into 108 HRUs. The importance of using threshold levels is to minimize the number of HRUs in the model and optimize it (66). Only a low threshold value of 5% was set for land use classes because maintaining the land use diversity was important.

Table 12. Slope classes

Slope classes	Area (km^2)	Area (%)
0-5 %	1774.44	19.89
5-15 %	3114.96	34.92
15-30 %	2924.19	32.78

30-45 %	977.76	10.96
>45 %	128.25	1.44

Sensitivity analysis. The purpose of the sensitivity analysis is to identify how much the selected parameters will impact the result of a model by varying the parameters (increasing or decreasing parameters' values) (26). In this study, the global sensitivity analysis for streamflow was performed using the SUFI-2 algorithm in SWAT-CUP for seventeen parameters that have the potential to influence the daily discharge. The most sensitive parameters were curve number (CN2), minimum depth of water in the shallow aquifer (GWQMN), baseflow alpha factor for bank storage (ALPHA_BNK), moist bulk density (SOL_BD), maximum canopy storage (CANMX), available water capacity of the soil layer (SOL_AWC), groundwater delay (GW_DELAY), and groundwater "revap" coefficient (GW_REVAP). The sensitivity of the seventeen parameters can be seen from Figure 13. The larger t-stat and smaller p-value indicate the more sensitive parameters.

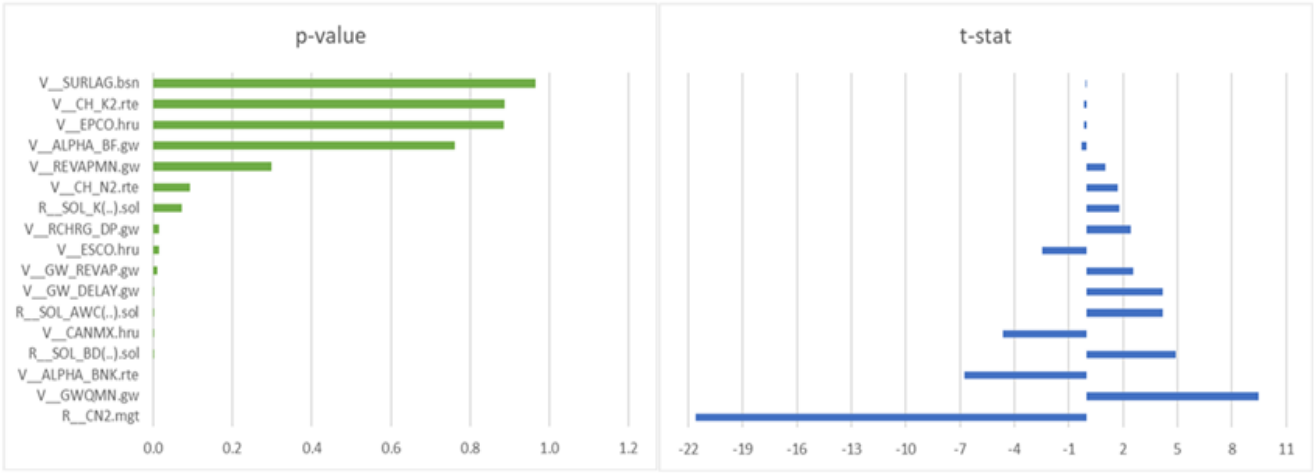

Figure 13. Sensitivity analysis

Model calibration and validation. The ArcSWAT model was run for sixteen years on a daily time step from 1st January, 2004 to 31st December, 2019, with a four-year warm-up period that means the model simulation period is twelve years starting in 2008, and ending in 2019. The warm-up period was used to stabilize the model with observed meteorological data. The ArcSWAT model was calibrated through the SUFI-2 algorithm in SWAT-CUP based on the LULC map of 2010 by adjusting the parameter range values to increase the correlation between the simulations and observations. The SWAT-CUP software was run for four iterations (800 simulations each) with the selected parameters for calibration. In the SWAT-CUP, new parameter ranges were recommended after each iteration and they were used in the next iteration. After four iterations, the model was

calibrated by reducing the curve number (CN2), available water capacity of the soil layer (SOL_AWC), increasing minimum depth of water in the shallow aquifer (GWQMN), moist bulk density (SOL_BD), maximum canopy storage (CANMX) and altering the other parameters (Table 13). The initial model simulation showed relatively high surface runoff; therefore, the existing CN2 value was reduced by 45 percent in all HRUs to decrease surface runoff. Also, the SOL_AWC value was decreased by 16 percent to increase baseflow. Moreover, the surface runoff lag coefficient value was adjusted at 5 days, which means the generated surface runoff enters the reach in a short period of time. The acceptable minimum and maximum values of parameters were set according to the SWAT manual (30).

Table 13. Model calibration

Parameters	Description	t-stat	p-value	Fitted value	Calibration range
R_CN2.mgt	SCS runoff curve number	-21.574	0.000	-0.45	-0.5-0.24
V_GWQMN.gw	Threshold depth of water in the shallow aquifer required for return flow to occur (mm)	9.500	0.000	2302.82	0-5000
V_ALPHA_BNK.rte	Baseflow alpha factor for bank storage (days)	-6.749	0.000	0.60	0-1
R_SOL_BD(..).sol	Moist bulk density	4.910	0.000	0.25	-0.5-0.6
V_CANMX.hru	Maximum canopy storage (mm)	-4.648	0.000	20.37	0-100
R_SOL_AWC(..).sol	Available water capacity of the soil layer	4.213	0.000	-0.16	-0.8-0.8
V_GW_DELAY.gw	Groundwater delay (days)	4.201	0.000	6.33	0-500
V_GW_REVAP.gw	Groundwater “revap” coefficient	2.574	0.010	0.15	0.02-0.2

V_ESCO.hru	Soil evaporation compensation factor	-2.453	0.014	0.97	0-1
V_RCHRG_DP.gw	Deep aquifer percolation fraction	2.446	0.015	0.23	0-1
R_SOL_K(..).sol	Saturated hydraulic conductivity	1.801	0.072	0.39	-0.8-0.8
V_CH_N2.rte	Manning's "n" value for the main channel	1.688	0.092	0.17	-0.01-0.3
V_REVAPMN.gw	Threshold depth of water in the shallow aquifer for "revap" to occur (mm)	1.041	0.298	616.65	0-1000
V_ALPHA_BF.gw	Baseflow alpha factor (days)	-0.303	0.762	0.15	0-1
V_EPCO.hru	Plant uptake compensation factor	-0.144	0.885	0.41	0-1
V_CH_K2.rte	Effective hydraulic conductivity in main channel alluvium	-0.144	0.886	197.75	-0.01-500
V_SURLAG.bsn	Surface runoff lag time	-0.043	0.966	5.72	0.05-24

v=replace, r=relative change: the existing parameters' values multiplied by (1+a given value).

The simulated results of discharge by means of the ArcSWAT model were compared with the observed data (lower) and in contrast to the precipitation (upper) at the Tuul-Altanbulag gauging station (Figure 14). The calibration of discharge is illustrated as a 95PPU graph in Figure 14. The calibrated model achieved P-factor of 0.5 and R-factor of 0.75, which means 50 percent of the measured discharge was bracketed by 95PPU within model prediction uncertainty. Overall, the simulation of discharge showed satisfactory agreement with the measurements with correlation coefficient (r) of 0.77 and 0.82, Nash-Sutcliffe efficiency coefficient (NSE) of 0.56 and 0.66 for the calibration (2008-2013) and validation (2014-2019) periods respectively. Moreover, the percentage bias (PBIAS) between the simulated and observed data was -10.3 which means the model overestimated the discharge. The simulated mean annual discharge was 11.18 m3/s and the observed mean annual discharge was 10.9 m3/s from 2008 to 2019 at the Tuul-Altanbulag gauging station (Table 14). The ArcSWAT model simulation results fall

under a satisfactory category (Table 15) according to the performance criteria of the model (58). However, some differences between measured and simulated discharge at a few time steps can be observed. These variations can be explained by human error during field measurement of streamflow and uneven distributions of weather stations within the study area. Furthermore, the calculated average annual precipitation was 264.6 mm, which falls within the measured range of 253-275 mm (45).

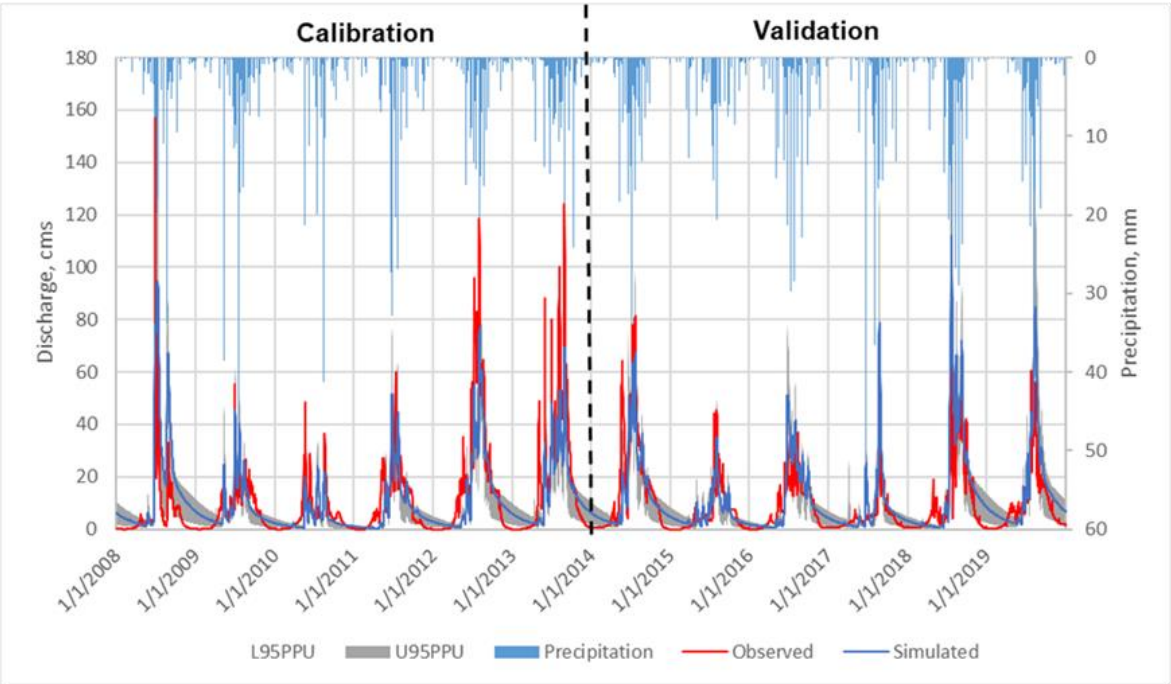

Figure 14. Observed and simulated daily discharge graph with 95PPU for calibration (2008-2013) and validation (2014-2019) periods.

Table 14. Performance of the model simulation

	r	NSE	PBIAS
Calibration (2008-2013)	0.77	0.56	-10.3
Validation (2014-2019)	0.82	0.66	-22

Table 15. General performance ratings of SWAT model (58)

Performance rating	NSE	PBIAS (%)
	Streamflow	
Very good	0.75 < NSE ≤ 1.00	PBIAS < ±10

Good	0.65 < NSE ≤ 0.75	±10 ≤ PBIAS < ±15
Satisfactory	0.50 < NSE ≤ 0.65	±15 ≤ PBIAS < ±25
Unsatisfactory	NSE ≤ 0.50	PBIAS ≥ ±25

Water quality simulation. The ArcSWAT model estimates the number of pollutants such as nitrogen, phosphorus, and nitrate within the basin. These contaminants are distributed from their sources through surface runoff and baseflow (30). In this study, monthly loadings of phosphorus and nitrate were simulated by the ArcSWAT model with LULC of 2010 (Figure 15). The water quality monitoring station near the Tuul-Alntanbulag gauging station was used to evaluate the model performance. According to observation data at Tuul-Altanbulag gauging station, nitrate levels are less than 1 mg/L with seasonal increases in the summer months and the phosphorus levels range between 0.05 and 0.41 mg/L. The correlation coefficients between simulated and measured nitrate and phosphorus were 0.81 and 0.74, respectively. The results of monthly simulations of nitrate and phosphorus adequately match with observed values.

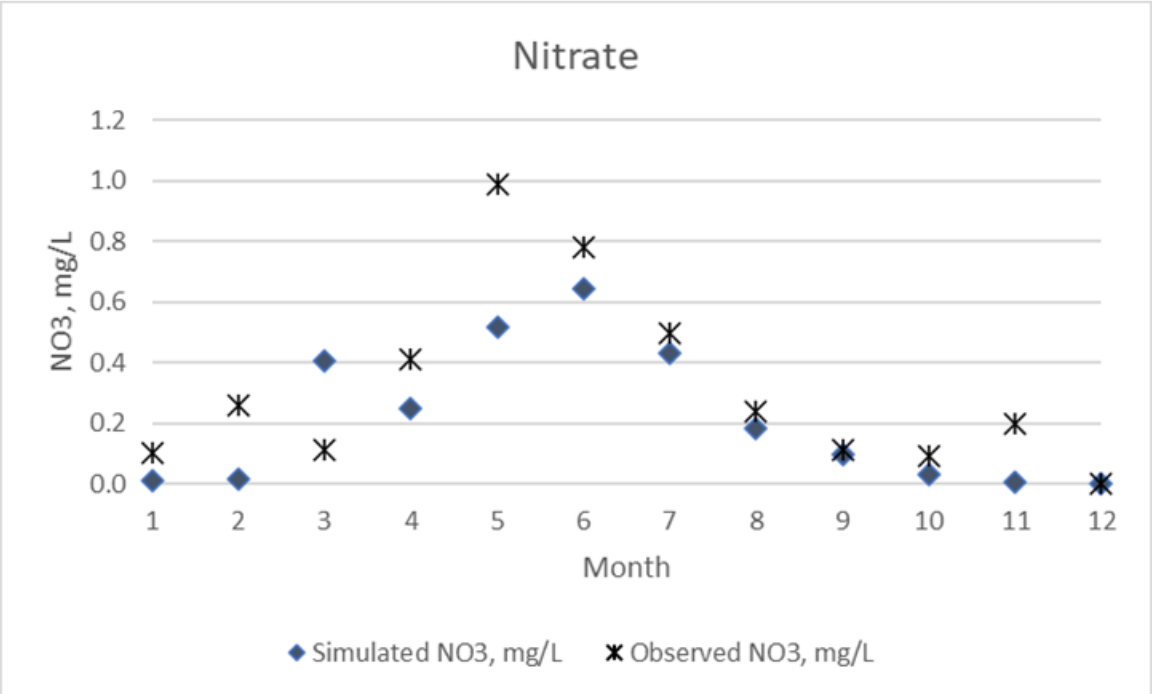

*SolP means soluble phosphorus.

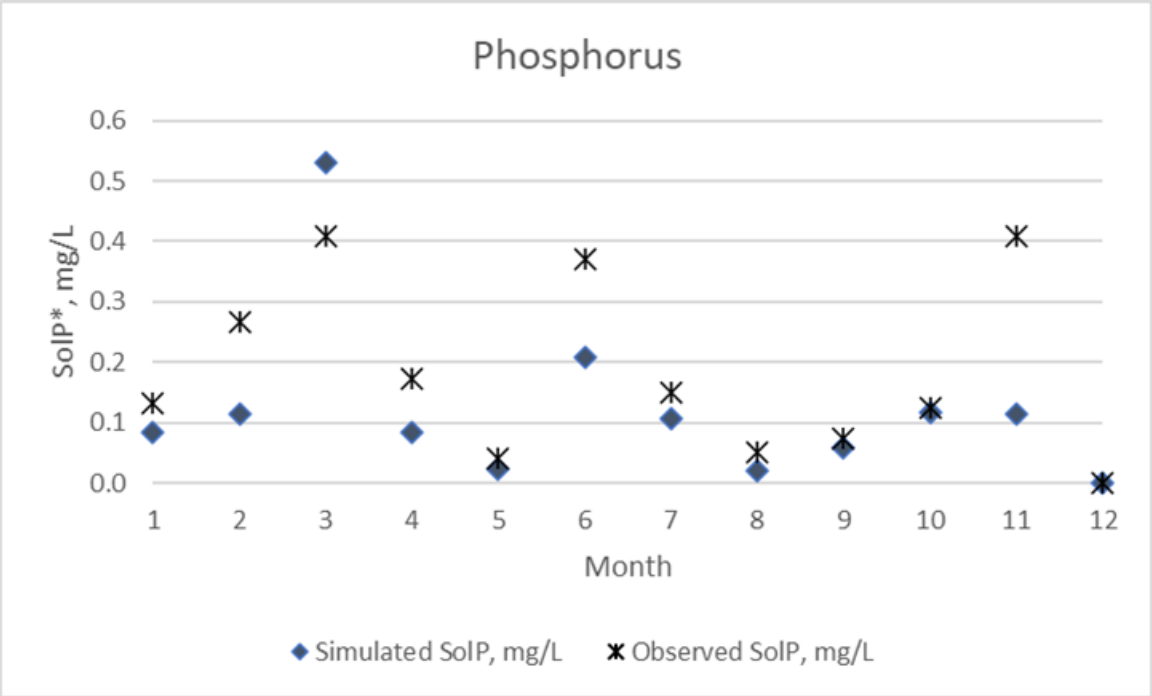

Figure 15. Observed and simulated monthly nitrate and phosphorus loads

The effect of land-use changes. In order to evaluate the effects of land-use changes on surface water quantity and quality for the Tuul river basin, two land-use maps in 2015 and 2019 were used as input data to the ArcSWAT model. The hydrological and water quality components are predicted separately at each HRU and routed through the hydrological network to the outlet (30). The HRU is the major influencing factor on discharge and nutrient concentration because it is created based on the soil, land use, and slope data. The numbers of HRUs are different for each LULC maps due to land use changes (Table 16).

Table 16. HRUs of LULC 2010, 2015, and 2019

	LULC 2010	**LULC 2015**	**LULC 2019**
HRUs	108	119	120

The dominant land use type was pasture land area (76% of the total study area in 2010). However, about 5 percent of pasture area was converted to urban areas in 2019. The urban area increased by 3 percent in 2019 compared to LULC of 2010 (see Table 7). The urban extension leads to land degradation. After calibrating the model with the best fitted parameters based on LULC map of 2010, the model was re-run with LULC maps of 2015 and 2019. As a result of land-use changes between 2010 and 2019 (Table 17),

surface runoff increased 1.6 percent, and lateral flow and water yield decreased 12.3 percent and 8.4 percent, respectively. Overall, the mean simulated streamflow decreased from 11.18 m^3/s in 2010 to 8.8 m^3/s in 2019.

Table 17. Effect of LULC changes on the hydrological components

	2010	**2015**	**2019**	**Change 2010-2019 (%)**
Precipitation, mm	308.9	308.9	308.9	-
Snowfall, mm	26.74	26.75	26.69	-0.05
Surface runoff, mm	0.57	1.52	2.18	1.61
Lateral flow, mm	19.94	7.84	7.68	-12.26
PET, mm	367.9	367.9	367.9	-
ET, mm	204.4	204.7	205.2	0.8
Water yield, mm	39.85	31.17	31.45	-8.4
Mean simulated discharge, m^3/s	11.18	8.72	8.8	-2.38

For the effects of land-use changes on water quality, annual nitrate and phosphorus loads are predicted to be increased. The annual nitrate and phosphorus loads have increased by 21.8 percent and 21.6 percent, respectively, under land-use changes between 2010 and 2019 (Table 18). These increments in loadings can be explained by the land degradation and increase in impervious surface area due to expansion of high-density urban areas. In high-density urban areas, sewage, road dust, road salt, application of fertilizer to vegetated areas in the street, household pet waste, and automobile detergents are the major sources of nitrate and phosphorus to waterways (67), (68). The pollutants are generated from their sources and cumulated in the impervious area. Then the cumulated pollutants are transported to a river via surface runoff. The results of model simulations with land-use changes from 2010 to 2019 showed the increase in surface runoff due to urbanization; hence the nitrate and phosphorus increased as well. The excess amount of phosphorus and nitrate causes eutrophication, which results in deterioration of water quality (67).

Table 18. Effect of LULC changes on water quality

	2010	**2015**	**2019**	**Change 2010-2019 (%)**
NO_3, mg/L	0.2171	0.2618	0.2645	21.8
SolP*, mg/L	0.1224	0.1436	0.1486	21.6

*SolP=soluble phosphorus

5. Conclusion

The main objective of this thesis was to evaluate the effects of land-use changes on surface water quality and quantity of the upper part of the Tuul river basin through the ArcSWAT hydrological model. To accomplish the main objective, the input data for the SWAT model were prepared and the model was calibrated and validated in the study area to increase the correlation between the simulation of the model and measured data. After calibration and validation, the impacts of land-use changes on the Tuul river surface water quantity and quality were analyzed from the model's simulation results.

For the input data, the land use classification maps (2010, 2015, and 2019) required for the model input data were classified by the supervised classification method using Landsat images, and the soil data were prepared based on the FAO international soil classification. Moreover, weather data were acquired from the National Agency for Meteorology, Hydrology and the Environmental Monitoring.

In the SWAT model, the Penman-Monteith approach was used for estimating potential evapotranspiration, whereas SCS curve number method was used to calculate surface runoff of each subbasin. The study area covers an area of 8919.6 km² which was subdivided into 6 subbasins with a total of 108 HRUs. The model simulation period was set from 2008 to 2019, with a calibration period from 2008 to 2013 (6 years) and a validation period from 2014-2019 (6 years). The simulation of the model was calibrated with LULC of 2010 by adjusting seventeen parameters using the SWAT-CUP software and daily observed discharge from 2008 to 2019. After calibration, the results of the model showed satisfactory performance for the simulation of streamflow and water quality. The simulated streamflow reasonably captured the measured values at the Tuul-Altanbulag gauging station with statistical results of 0.77 (*r*) and 0.56 (NSE) for calibration period, and 0.82 (*r*) and 0.66 (NSE) for validation period.

In this study, different land-use maps with 119 HRUs for 2015, and 120 HRUs for 2019 were inputted into the ArcSWAT model to evaluate the impacts of land-use changes on discharge and water quality of the upper part of the Tuul river basin. After running the model with different LULC maps, the results showed that land-use changes lead to an increase in surface runoff, and nitrate and phosphorus loads. Contrastingly, streamflow decreased from 11.18 m^3/s to 8.8 m^3/s due to the rapid urbanization between 2010 and 2019. For assessing the effect of LULC changes on water quality, phosphorus and nitrate content in the streamflow was simulated at a monthly time scale by the ArcSWAT model. The simulation showed an appropriate model performance with correlation coefficient of 0.81 and 0.74 for nitrate and phosphorus, respectively.

In conclusion, the simulation results of the ArcSWAT hydrological model proved that this model is applicable in evaluating the effects of land-use changes on surface water quality and quantity in Mongolian semi-arid region. Policymakers could use the outcomes of the study as a decision-making tool in developing a proper land use management. Because streamflow and water quality tend to be very sensitive to land-use changes.

6. Reference

1. Tchakerian VP. HYDROLOGY, FLOODS AND DROUGHTS | Deserts and Desertification. In: Encyclopedia of Atmospheric Sciences. Elsevier; 2015. p. 185–92.
2. Albertson JD, Kiely G. On the structure of soil moisture time series in the context of land surface models. Journal of Hydrology. 2001 Mar;243(1–2):101–19.
3. National statistical organization. Mongolian water resources and use. 2017.
4. Ministry of environment and green development (MEGD). Tuul river basin integrated water resource management. Ulaanbaatar. 2012.
5. Asian Development Bank. Overview of Mongolia's water resources system and management. 2020.
6. Byambakhuu I, BSh, UP, MZ. Mongolia Water-Green growth scenarios. Ulaanbaatar. 2016.
7. National statistical organization. Mongolian population. 2020.
8. Dolgorsuren G W van der LCN. Tuul river basin integrated water management plan. 2012.
9. Enkhjargal T. OD. Results of a study determining the Tuul river water quality and pollution level. 2017.
10. Altansukh O. Surface water quality assessment and modelling a case study in the Tuul river. Ulaanbaatar. 2010.
11. Altantsetseg G. Water pollution in the Tuul river and influencing factors. 2015.
12. Environmental department M of U. Climate change mitigation and adaptation sub-program. Ulaanbaatar. 2018.
13. Yang Q, Zhang X. Improving SWAT for simulating water and carbon fluxes of forest ecosystems. Science of The Total Environment. 2016 Nov;569–570:1478–88.
14. Shinde VT, Tiwari KN, Nandgude SB, Singh M. Water Quality Assessment and Application of SWAT Model for Hydrologic Simulations in a Mined Watershed. Climate Change and Environmental Sustainability. 2017;5(2):111.

15. Talib A, Randhir TO. Climate change and land use impacts on hydrologic processes of watershed systems. Journal of Water and Climate Change. 2017 Sep 1;8(3):363–74.

16. Marshall E, Randhir TO. Spatial modeling of land cover change and watershed response using Markovian cellular automata and simulation. Water Resources Research. 2008 Apr;44(4).

17. Arnold JG, Srinivasan R, Muttiah RS, Williams JR. LARGE AREA HYDROLOGIC MODELING AND ASSESSMENT PART I: MODEL DEVELOPMENT. J Am Water Resour Assoc. 1998 Feb;34(1):73–89.

18. Khoi DN, Nguyen V, Sam TT, Nhi P. Evaluation on Effects of Climate and Land-Use Changes on Streamflow and Water Quality in the La Buong River Basin, Southern Vietnam. Sustainability. 2019 Dec 16;11(24):7221.

19. El-Khoury A, Seidou O, Lapen DR, Que Z, Mohammadian M, Sunohara M, et al. Combined impacts of future climate and land use changes on discharge, nitrogen and phosphorus loads for a Canadian river basin. Journal of Environmental Management. 2015 Mar; 151:76–86.

20. Chotpantarat S, Boonkaewwan S. Impacts of land-use changes on watershed discharge and water quality in a large intensive agricultural area in Thailand. Hydrological Sciences Journal. 2018 Jul 4;63(9):1386–407.

21. Mehdi B, Ludwig R, Lehner B. Evaluating the impacts of climate change and crop land use change on streamflow, nitrates and phosphorus: A modeling study in Bavaria. Journal of Hydrology: Regional Studies. 2015 Sep; 4:60–90.

22. Gyawali B, Shrestha S, Bhatta A, Pokhrel B, Cristan R, Antonious G, et al. Assessing the Effect of Land-Use and Land-Cover Changes on Discharge and Sediment Yield in a Rural Coal-Mine Dominated Watershed in Kentucky, USA. Water (Basel). 2022 Feb 9;14(4):516.

23. Saddique N, Mahmood T, Bernhofer C. Quantifying the impacts of land use/land cover change on the water balance in the afforested River Basin, Pakistan. Environmental Earth Sciences. 2020 Oct 23;79(19):448.

24. Wilson CO, Weng Q. Simulating the impacts of future land use and climate changes on surface water quality in the Des Plaines River watershed, Chicago Metropolitan Statistical Area, Illinois. Science of The Total Environment. 2011 Sep;409(20):4387–405.

25. Kumar M, Denis DM, Kundu A, Joshi N, Suryavanshi S. Understanding land use/land cover and climate change impacts on hydrological components of Usri watershed, India. Applied Water Science. 2022 Mar 11;12(3):39.

26. Byambakhuu I. Study of Eco-hydrological Responses to Global Warming and Grazing Pressure in Mongolian Semi-arid Region. Dissertation. University of Tsukuba, Japan. 2011.

27. Davaasuren D. Estimation of Land use impact on Tuul river surface runoff using HEC-HMS modeling system. 2015.

28. Purevsuren M. Modeling assessment of Tuul river surface runoff and quality. 2018.

29. Norvanchig J, Randhir TO. Simulation of ecohydrological processes influencing water supplies in the Tuul River watershed of Mongolia. Journal of Hydroinformatics. 2021 Sep 1;23(5):1130–45.

30. Neitsch SL; AJG; KJR; WJR. Soil and Water Assessment Tool Theoretical Documentation Version 2009. Texas: Texas Water Resources Institute, Temple; 2011.

31. R. A. Leonard, W. G. Knisel, D. A. Still. GLEAMS: Groundwater Loading Effects of Agricultural Management Systems. Transactions of the ASAE. 1987;30(5):1403–18.

32. Knisel WG. CREAMS, a field scale model for chemicals, runoff and erosion from agricultural management systems. Vol. Volume1. USDA Conservation Research; 1980. 643 p.

33. J. R. Williams, C. A. Jones, P. T. Dyke. A Modeling Approach to Determining the Relationship Between Erosion and Soil Productivity. Transactions of the ASAE. 1984;27(1):0129–44.

34. Brown LC and TOBJr. The enhanced water quality model QUAL2E and QUAL2E-UNCAS documentation and user manual. 1987. 3–87 p.

35. Arnold JG; KJR; SR; WJR; HEB; NSL. Input/Output Documentation Version 2012. Texas: Texas Water Resources Institute; 2012.

36. USDA Soil Conservation Service. National Engineering Handbook Section 4 Hydrology. 1972.

37. Heber Green W, Ampt GA. Studies on Soil Phyics, Part 1, the Flow of Air and Water through Soils. The Journal of Agricultural Science. 1911 May 27;4(1):1–24.

38. Mein RG, Larson CL. Modeling infiltration during a steady rain. Water Resources Research. 1973 Apr;9(2):384–94.

39. Allen RG, Jensen ME, Wright JL, Burman RD. Operational Estimates of Reference Evapotranspiration. Agronomy Journal. 1989 Jul;81(4):650–62.

40. Allen RG. A Penman for All Seasons. Journal of Irrigation and Drainage Engineering. 1986 Nov;112(4):348–68.

41. Monteith JL. Evaporation and the environment. The state and movement of water in living organisms. Cambridge Univ. Press, London, U.K; 1965. 205–234 p.

42. PRIESTLEY CHB, TAYLOR RJ. On the Assessment of Surface Heat Flux and Evaporation Using Large-Scale Parameters. Monthly Weather Review. 1972 Feb;100(2):81–92.

43. George H. Hargreaves, Zohrab A. Samani. Reference Crop Evapotranspiration from Temperature. Applied Engineering in Agriculture. 1985;1(2):96–9.

44. Ritchie JT. Model for predicting evaporation from a row crop with incomplete cover. Water Resources Research. 1972 Oct;8(5):1204–13.

45. Javzandorj L. OD, UG et al., Tuul River: Ecological change and water management. 2011.

46. Dalai S, Dambaravjaa O, Purevjav G. Water Challenges in Ulaanbaatar, Mongolia. In 2019. p. 347–61.

47. U.S. Department of Agriculture (USDA). United States Department of Agriculture, National Agricultural Statistics Service. 2011.

48. Mohammady M, Moradi HR, Zeinivand H, Temme AJAM. A comparison of supervised, unsupervised and synthetic land use classification methods in the north of Iran. International Journal of Environmental Science and Technology. 2015 May 16;12(5):1515–26.

49. Abbaspour KC. Swat-cup 2012. SWAT calibration and uncertainty program—A user manual. 2013.

50. Hosseini SH, Khaleghi MR. Application of SWAT model and SWAT-CUP software in simulation and analysis of sediment uncertainty in arid and semi-arid watersheds (case study: the Zoshk–Abardeh watershed). Modeling Earth Systems and Environment. 2020 Dec 18;6(4):2003–13.

51. Khatun S, Sahana M, Jain SK, Jain N. Simulation of surface runoff using semi distributed hydrological model for a part of Satluj Basin: parameterization and global sensitivity analysis using SWAT CUP. Modeling Earth Systems and Environment. 2018 Sep 26;4(3):1111–24.

52. Ha L, Bastiaanssen W, van Griensven A, van Dijk A, Senay G. Calibration of Spatially Distributed Hydrological Processes and Model Parameters in SWAT Using Remote Sensing Data and an Auto-Calibration Procedure: A Case Study in a Vietnamese River Basin. Water (Basel). 2018 Feb 16;10(2):212.

53. Beven K, Binley A. The future of distributed models: Model calibration and uncertainty prediction. Hydrological Processes. 1992 Jul;6(3):279–98.

54. Alamirew CD. Modeling of Hydrology and Soil Erosion in Upper Awash River Basin. University of Bonn, Institut für Städtebau, Bode-nordnung und Kulturtechnik; 2006. 235 p.

55. Abbaspour KC, Johnson CA, van Genuchten MTh. Estimating Uncertain Flow and Transport Parameters Using a Sequential Uncertainty Fitting Procedure. Vadose Zone Journal. 2004 Nov;3(4):1340–52.

56. Abbaspour KC, Yang J, Maximov I, Siber R, Bogner K, Mieleitner J, et al. Modelling hydrology and water quality in the pre-alpine/alpine Thur watershed using SWAT. Journal of Hydrology. 2007 Feb;333(2–4):413–30.

57. Abbaspour K, Vaghefi S, Srinivasan R. A Guideline for Successful Calibration and Uncertainty Analysis for Soil and Water Assessment: A Review of Papers from the 2016 International SWAT Conference. Water (Basel). 2017 Dec 22;10(1):6.

58. D. N. Moriasi, J. G. Arnold, M. W. Van Liew, R. L. Bingner, R. D. Harmel, T. L. Veith. Model Evaluation Guidelines for Systematic Quantification of Accuracy in Watershed Simulations. Trans ASABE. 2007;50(3):885–900.

59. J. G. Arnold, D. N. Moriasi, P. W. Gassman, K. C. Abbaspour, M. J. White, R. Srinivasan, et al. SWAT: Model Use, Calibration, and Validation. Trans ASABE. 2012;55(4):1491–508.

60. Nash JE, Sutcliffe JV. River flow forecasting through conceptual models part I — A discussion of principles. Journal of Hydrology. 1970 Apr;10(3):282–90.

61. Gupta HV, Sorooshian S, Yapo PO. Status of Automatic Calibration for Hydrologic Models: Comparison with Multilevel Expert Calibration. Journal of Hydrologic Engineering. 1999 Apr;4(2):135–43.

62. Congalton RG. A review of assessing the accuracy of classifications of remotely sensed data. Remote Sensing of Environment. 1991 Jul;37(1):35–46.

63. Tilahun A. Accuracy Assessment of Land Use Land Cover Classification using Google Earth. American Journal of Environmental Protection. 2015;4(4):193.

64. Stehman S v. Sampling designs for accuracy assessment of land cover. International Journal of Remote Sensing. 2009 Sep 23;30(20):5243–72.

65. Leta MK, Demissie TA, Tränckner J. Modeling and Prediction of Land Use Land Cover Change Dynamics Based on Land Change Modeler (LCM) in Nashe Watershed, Upper Blue Nile Basin, Ethiopia. Sustainability. 2021 Mar 27;13(7):3740.

66. Winchell M; SR; DLM; AJ. ArcSWAT Interface for SWAT2012. User's Guide. Texas; 2013.

67. Hobbie SE, Finlay JC, Janke BD, Nidzgorski DA, Millet DB, Baker LA. Contrasting nitrogen and phosphorus budgets in urban watersheds and implications for managing urban water pollution. Proceedings of the National Academy of Sciences. 2017 Apr 18;114(16):4177–82.

68. Yang YY, Toor GS. Stormwater runoff driven phosphorus transport in an urban residential catchment: Implications for protecting water quality in urban watersheds. Scientific Reports. 2018 Dec 3;8(1):11681.

7. Appendix

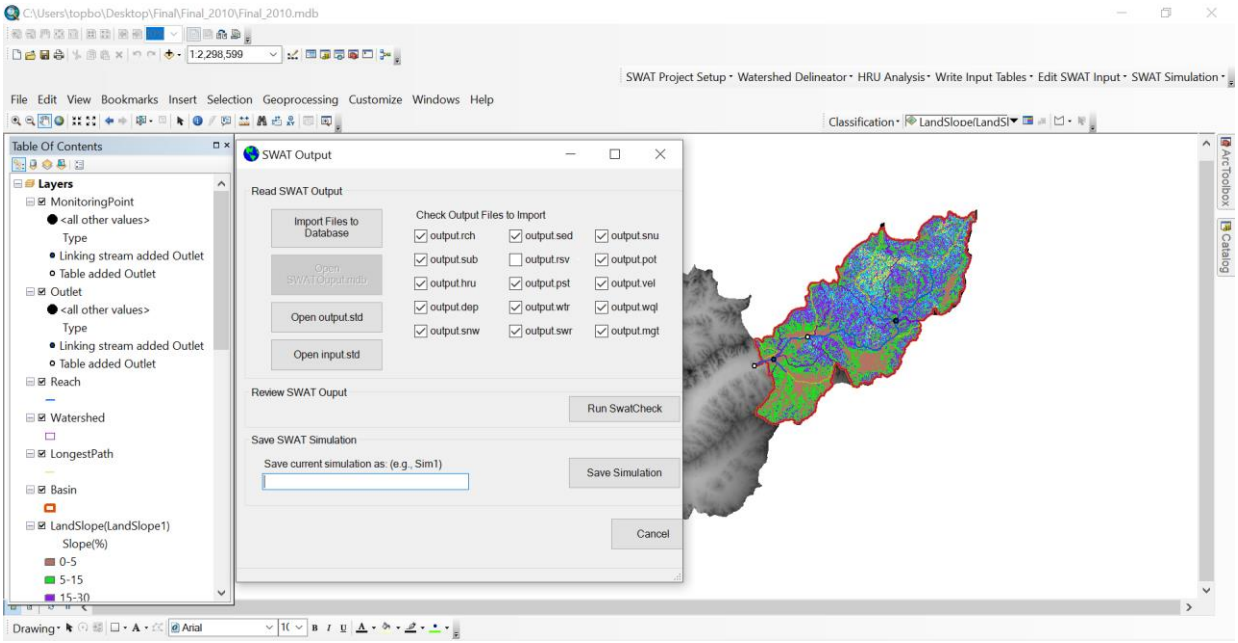

Figure 16. The simulation of ArcSWAT model

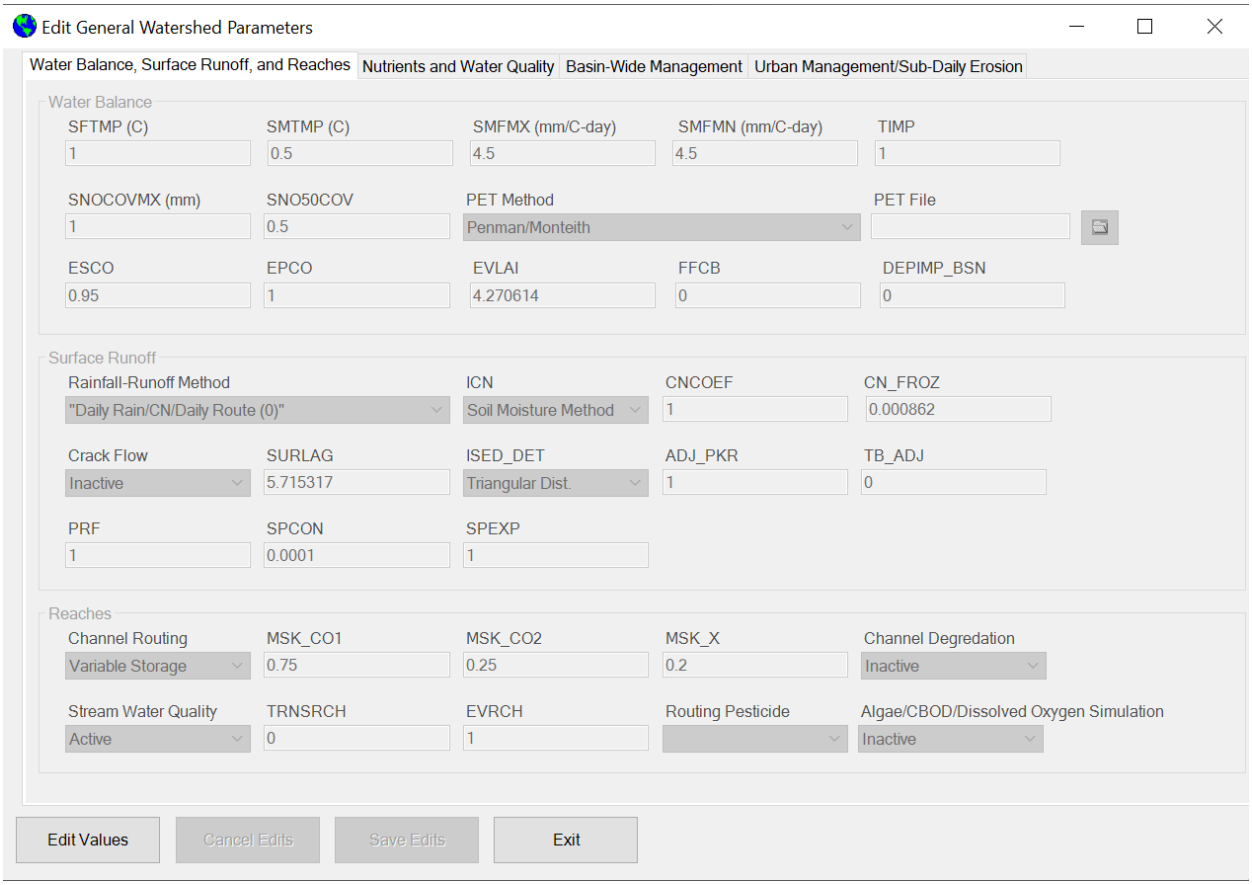

Figure 17. Inserting the calibrated parameters into the model